Application of direct-fitting, mass-integral, and multi-rate methods to analysis of flowing fluid electric conductivity logs from Horonobe, Japan

Christine Doughty and Chin-Fu Tsang

Earth Sciences Division
Lawrence Berkeley National Laboratory
Berkeley, California 94720, USA

Koichiro Hatanaka, Satoshi Yabuuchi and Hiroshi Kurikami[1]

Horonobe Underground Research Unit
Japan Atomic Energy Agency
Horonobe-cho, Teshio-gun, Hokkaido, 098-3224, Japan

August 2007

Abstract

The flowing fluid electric conductivity (FFEC) logging method is an efficient way to provide information on the depths, salinities, and transmissivities of individual conductive features intercepted by a borehole, without the use of specialized probes. Using it in a multiple-flow-rate mode allows, in addition, an estimate of the inherent "far-field" pressure heads in each of the conductive features. The multi-rate method was successfully applied to a 500-m borehole in a granitic formation and reported recently. The present paper presents the application of the method to two zones within a 1000-m borehole in sedimentary rock, which produced, for each zone, three sets of logs at different pumping rates, each set measured over a period of about one day. The data sets involve a number of complications, such as variable well diameter, free water table decline in the well, and effects of drilling mud. To analyze data from this borehole, we apply various techniques that have been developed for analyzing FFEC logs: direct-fitting, mass-integral, and the multi-rate method mentioned above. In spite of

[1] Current address: Nuclear Waste Management Organization of Japan (NUMO), 1-23, Shiba 4-chome, Minato-ku, Tokyo 108-0014, Japan

complications associated with the tests, analysis of the data is able to identify 44 hydraulically conducting fractures distributed over the depth interval 150-775 meters below ground surface. The salinities (in FEC), and transmissivities and pressure heads (in dimensionless form) of these 44 features are obtained and found to vary significantly among one another. These results are compared with data from eight packer tests with packer intervals of 10-80 m, which were conducted in this borehole over the same depth interval. They are found to be consistent with these independent packer-test data, thus demonstrating the robustness of the FFEC logging method under non-ideal conditions.

1. Introduction

Knowledge of the locations and hydraulic properties of conductive features is needed for understanding flow and transport through fractured rocks. Boreholes drilled deep into the rock are often employed to obtain this information. Various downhole methods for studying fracture flow have been developed over the past few decades. Coring and geophysical methods may be able to identify the fractures themselves, but they are unlikely to provide direct information on fracture flow properties. Straddle-packer pump-testing yields fracture flow properties, but is very time-consuming and expensive. Flow-logging techniques are an attractive alternative – they measure flow directly and are efficient to deploy in the field. Several varieties of flow logging exist, including spinner surveys, heat-pulse flow meters (Paillet and Pedler, 1996; Öhberg and Rouhiainen, 2000), tracer dilution analysis (Brainerd and Robbins, 2004), and the flowing fluid electric conductivity (FFEC) logging method, sometimes referred to as hydrophysical logging, the technique employed in the present study.

In the FFEC logging method, wellbore fluid is replaced with de-ionized water or water of constant salinity different from that of the formation water. Then FEC profiles in the wellbore are measured at a series of times while the well is pumped at a constant rate. Locations where native fluid enters the wellbore show peaks in the FFEC logs. By fitting the growth and movement of these peaks with a numerical model, one can infer inflow strengths and salinities of individual permeable features intersected by the

borehole. Since Tsang et al. (1990) introduced the method, it has been widely applied in deep wells down to 1500 m or more (Kelley et al., 1991; Guyonnet et al., 1993; Doughty et al., 2005), in inclined boreholes drilled in the underground Grimsel Test Laboratory (Marschall and Vomvoris, 1995), and extensively in shallower wells down to about 100 m (Evans et al., 1992; Pedler et al., 1992; Bauer and LoCoco, 1996; Paillet and Pedler, 1996; Karasaki et al., 2000). Continued development of analytical and numerical data-analysis techniques (Löw et al., 1994; Evans, 1995; Tsang and Doughty, 2003; Doughty and Tsang, 2005) have broadened the range of applicability and enhanced the ease of use of the method. Note that FFEC logging requires little or no specialized equipment or expertise, and may be carried out more quickly than most other methods, making it a valuable tool for efficient subsurface characterization.

Data analysis techniques include three main methods. First, the direct fitting of the time-series of FFEC profiles yields the locations, inflow strengths, and salinities of permeable features (Tsang et al., 1990). Second, integrating the FFEC profiles over the entire logged interval (the so-called mass-integral or $M(t)$ method) provides an estimate of salt mass in place as a function of time, which facilitates the analysis (Doughty and Tsang, 2005). Third, if FFEC logging is repeated using two different well pumping rates (a procedure known as multi-rate FFEC logging), then the transmissivities and inherent pressure heads of the different permeable features can also be determined (Tsang and Doughty, 2003).

Direct-fitting and multi-rate analyses for FFEC logging were recently carried out successfully for a 500-m deep borehole in fractured granitic rock in the Tono region of Japan (Doughty et al., 2005). The analyses identified 19 hydraulically conducting fractures, which showed a range of values for transmissivity, salinity, and pressure head. Using three different pumping rates allowed analysis of three alternative combinations of two pumping-rate data sets, providing a consistency check on the multi-rate analysis. Good comparisons against static FEC profiles and against independent chemical, geological, and hydrogeological data further enhanced confidence in the FFEC logging method.

The present paper describes a field application of the multi-rate FFEC logging method, using data from a 1,000-meter deep well known as Well HDB-11, in fractured sedimentary rock in the Horonobe area of Japan. This case differs from the Tono application (Doughty et al., 2005) in several significant ways. Not only is the rock sedimentary instead of granitic, but also a number of complications are associated with the logging data, including

- a section of the borehole having a variable wellbore diameter
- the presence of a free water surface in the borehole (i.e., the logged zone is not isolated with packers)
- flow of low-salinity water into fractures during the initial recirculation period
- periods of unknown pumping rate during FFEC logging
- a small increase in salinity all along the borehole during FFEC logging, probably the result of residual mud used in drilling the well
- a gradual borehole pressure decline during FFEC logging
- possible unknown inflows into the borehole from unmonitored borehole sections
- sets of FFEC profiles that are not all internally consistent

Whereas the Tono application demonstrated the first field application of the multi-rate FFEC logging method, the present application examines the robustness of the method under non-ideal conditions.

Section 2 describes the basic method. Section 3 shows the geological setting, the field test set-up, measurement procedure, and data. Sections 4 and 5 explain the various analysis methods used to deal with all the data complications, and present the results. Section 6 compares the results with independent data from packer tests that have been conducted in Well HDB-11. Section 7 discusses a number of issues arising from the analysis, and finally Section 8 provides concluding remarks and recommendations for improving future field procedures.

2. Summary of the Method

This section gives a summary of data collection and analysis methods. Details of the data collection method may be found in Doughty et al. (2005). Details of the analysis method may be found in Tsang et al. (1990), Tsang and Doughty (2003), and Doughty and Tsang (2005).

2.1 Data Collection

In the FFEC logging method, the wellbore water is first replaced by de-ionized water or, alternatively, by water of a constant salinity distinctly different from that of the formation water. This is done by passing de-ionized water down a tube to the bottom of the wellbore at a low rate, while simultaneously pumping from the top of the well at the same rate. The goal is to completely replace the wellbore water with de-ionized water without pushing any de-ionized water out into the rock formation. The FEC of the effluent is monitored throughout wellbore water replacement, which continues until a low stable FEC value is reached. Next, the well is shut in and the de-ionized water tube is removed. Then the well is pumped from the top at a constant low flow rate Q_1 (e.g., several or tens of liters per minute), while an electric conductivity probe is lowered into the wellbore to scan the FEC as a function of depth. This produces what is known as a flowing FEC (or FFEC) log or profile. With constant pumping conditions, a series of five or six FFEC logs are typically obtained over a one- or two-day period. Optionally, the entire procedure may be repeated using a different pumping rate Q_2, typically half or double the original rate Q_1. Throughout the process, the water level in the well should be monitored.

2.2 Data Analysis

At depth locations where native water enters the wellbore (inflow feed points), the FFEC logs display peaks. These peaks grow with time and are skewed in the direction of water flow. By analyzing these logs as described below, it is possible to obtain the inflow rates and salinities of groundwater inflow from the individual feed points. Although locations where water leaves the wellbore (outflow feed points) do not produce distinct peaks in the FFEC logs, they can sometimes be identified by their impact on

other peaks using a mass-integral method (Doughty and Tsang, 2005). By performing FFEC logging using different pumping rates, a procedure called multi-rate FFEC logging (Tsang and Doughty, 2003), the inherent pressure heads and transmissivities of the permeable features giving rise to the feed points can also be determined.

The numerical models BORE (Hale and Tsang, 1988) and the enhanced version BORE II (Doughty and Tsang, 2000) calculate the time evolution of ion concentration (salinity) through the wellbore by solving the one-dimensional advection-dispersion equation, given a pumping rate Q and a set of feed-point locations z_i, strengths q_i, and salinities C_i (i.e., the forward problem) . Fluid flow in the wellbore is considered quasi-steady: that is, fluid is assumed to be incompressible so it responds instantly to changes in pumping rate or feed-point strength. Density differences between the original wellbore fluid (de-ionized or low-salinity water, which may contain traces of drilling mud) and formation fluid flowing into the wellbore are neglected (another version of the code, VHBORE (Hale and Tsang, 1994) does consider compressible flow with compositional density differences, but it is not employed here). The governing equations for BORE II are presented in Doughty and Tsang (2005). Some analytical solutions are available for FFEC profiles obtained from simple feed-point configurations (e.g., Drost et al., 1968; Tsang et al., 1990), but BORE II broadens the range of applicability of the analytical solutions by considering multiple inflow and outflow feed points, isolated and overlapping FEC peaks, early-time and late-time behavior, time-varying feed-point strengths and salinities, as well as the interplay of advection and dispersion in the wellbore.

The general procedure for using BORE II is to estimate feed-point locations z_i by examining early-time FFEC profiles, then assign feed-point properties (q_i and C_i) by trial and error until an acceptable match between modeled and observed FFEC profiles is obtained (i.e., an inverse problem). Integrating the FFEC profiles over the entire logged interval or a desired sub-interval provides an estimate of salt mass in the borehole interval under study as a function of time, which provides a useful constraint for the analysis. If FFEC logs were only collected using one pumping rate Q, then the analysis ends here.

185 However, if multiple sets of FFEC logs are available, the inverse procedure is repeated
186 for each value of Q, with the inverse problems constrained by requiring that the same set
187 of z_i and C_i values be used for each one.
188
189 Assuming that two sets of FFEC logs were collected with pumping rates Q_1 and Q_2,
190 and that the strengths of individual feed points i, as evaluated by BORE II, are $q_i^{(1)}$ and
191 $q_i^{(2)}$ respectively, then Tsang and Doughty (2003) showed that

192 $$\frac{T_i}{T_{tot}} = \frac{q_i^{(1)} - q_i^{(2)}}{Q_1 - Q_2} \qquad (1)$$

193 and

194 $$\frac{(P_i - P_{avg})}{(P_{avg} - P_{wb}^{(1)})} = \frac{q_i^{(1)}/Q_1}{T_i / T_{tot}} - 1\,, \qquad (2)$$

195 where T_i/T_{tot} is the fraction of the total transmissivity of the logged interval corresponding
196 to the fracture or permeable zone represented by the ith feed point ($\Sigma T_i/T_{tot} = 1$); P_i is the
197 inherent pressure head of fracture i; P_{avg} is the pressure in the wellbore when it is shut-in
198 for an extended time, which can be calculated as a transmissivity-weighted average over
199 all fracture pressures: $P_{avg} = \Sigma(T_i P_i)/T_{tot}$; and $P_{wb}^{(1)}$ is the pressure drawdown in the
200 wellbore during the FFEC logging at $Q = Q_1$. The derivation of Equations (1) and (2)
201 assumes that the flow geometries within all the hydraulically conductive fractures
202 intersecting the borehole are the same (e.g., all radial flow or all linear flow). For
203 example, for radial steady flow, one can write

204 $$q_i = \frac{2\pi T_i (P_i - P_{wb})}{\ln(r_i / r_{wb})}, \qquad (3)$$

205 where r_i is the radial distance beyond which pressure changes due to pumping are small
206 and r_{wb} is the wellbore radius. With all fractures having the same r_i value, Equation (3)
207 can be readily summed over all i feed points to yield

208 $$Q = \frac{2\pi T_{tot} (P_{avg} - P_{wb})}{\ln(r_i / r_{wb})}\,. \qquad (4)$$

209 The inherent pressure head P_i is the ambient or undisturbed pressure in a fracture (or
210 permeable layer) that the borehole intersects, and it is the value that would be measured

under non-pumping conditions with packers inflated in the wellbore on either side of the fracture to isolate it for a substantial time period to attain steady-state pressure conditions. In contrast, P_{avg} is the value that would be measured under non-pumping conditions when the wellbore has been open to all feed points in the logged interval for a substantial time period. The pressure difference P_i - P_{avg} provides a measure of the driving force for fluid flow between hydraulically conducting fractures and the wellbore under non-pumping or shut-in conditions, which gives rise to internal wellbore flow. Note that from the definition of P_{avg} above, if all the P_i values are the same, then $P_i = P_{avg}$, and there will be no internal wellbore flow under non-pumping conditions. In this case, Equation (2) shows that feed-point strength q_i is proportional to fracture transmissivity T_i.

The ratios on the left-hand-sides of Equations (1) and (2) are the fundamental results of a multi-rate analysis. If T_{tot}, P_{avg}, and P_{wb} are also known (say from a conventional well test of the entire well section), then the T_i and P_i values themselves can be directly calculated. Additionally, because T_i and P_i appear in ratios in Equations (1) and (2), if one particular set of T_j and P_j are measured (say from a well test on a packed-off interval across fracture j), then all the additional T_i and P_i values can also be determined.

Tsang and Doughty (2003) denoted the group on the left-hand-side of Equation (2) as the normalized pressure head difference, $(\Delta P)_n$. Note that the denominator of $(\Delta P)_n$ depends on Q_1 through $P_{wb}^{(1)}$. This Q dependence becomes inconvenient if several pairs of tests using different values of Q are to be compared. Hence, both sides of Equation (2) are multiplied by Q_1

$$\frac{P_i - P_{avg}}{P_{avg} - P_{wb}^{(1)}} Q_1 = \left(\frac{q_i^{(1)} / Q_1}{T_i / T_{tot}} - 1 \right) Q_1 . \qquad (5)$$

The ratio $Q_1/(P_{avg} - P_{wb}^{(1)})$ on the left-hand-side is known in the petroleum literature as the productivity index I, defined as the ratio of pumping rate to drawdown during a well test. I characterizes the well and the permeable formation it intersects, and is independent of Q. Defining $(P_i - P_{avg}) = \Delta P_i$, Equation (3) becomes

239 $$I\Delta P_i = \left(\frac{q_i^{(1)} / Q_1}{T_i / T_{tot}} - 1 \right) Q_1 \quad . \tag{6}$$

240 The quantity $I\Delta P_i$, provides a measure of inherent pressure head for the ith feed point that
241 is independent of Q.
242
243 The multi-rate analysis requires two sets of FFEC logs at two pumping rates (at Q and
244 $2Q$, for example), but if three sets of logs for three pumping rates, Q_1, Q_2 and Q_3 are
245 available, then three sets of results can be obtained by analyzing three combinations of
246 data sets: (Q_1 and Q_2), (Q_2 and Q_3) and (Q_3 and Q_1). This permits internal checking, a
247 means to evaluate measurement errors, and an estimate on the confidence level of the
248 analysis results.
249

250 # 3. Horonobe Well HDB-11 Data

251 Horonobe town is located in the northernmost part of Hokkaido, Japan (**Figure 1**).
252 The main subsurface investigation area is about 3 km x 3 km square, including an
253 underground research laboratory (URL) construction site, which is located about 15 km
254 from the present coast line of the Japan Sea. The gentle topography is thought to be a
255 periglacial landform. Horonobe town overlies Neogene sedimentary sequences (in
256 ascending order: Souya coal-bearing Formation, Masuhoro Formation, Wakkanai
257 Formation, Koetoi Formation, and Yuchi Formation), which are underlain by an igneous
258 and Palaeogene-to-Cretaceous sedimentary basement (**Figure 2**). The Wakkanai and
259 Koetoi Formations, which are Neogene argillaceous sedimentary formations, are the
260 formations intercepted by Well HDB-11; they are also the host rocks for the URL. The
261 area is tectonically active and micro-earthquake swarms have occasionally occurred in
262 and around Horonobe town. The Eastern margin of the Japan Sea is a well-defined
263 seismic zone, especially for micro-earthquakes. The Omagari Fault (**Figure 2**) was
264 active until early Quaternary times and is believed to have a maximum vertical
265 displacement of over 1000 m. Present-day active faults are thought to occur to the west
266 of the Omagari Fault. In addition, historical coal mines were present in Horonobe town,

and oil/gas exploration work including deep borehole investigations has been conducted in the region.

Well HDB-11 was drilled in four stages, as shown in **Figure 3**. FFEC logs were taken after the second stage, drilling from 150 – 450 m through the Koetoi Formation (herein denoted the shallow zone), and after the third stage, drilling from 450 m – 800 m through the Wakkanai Formation (herein denoted the deep zone). During each logging period, the well was cased from the surface to the top of the logged zone, leaving the logged zone uncased. During recirculation periods, shallow groundwater with very low electrical conductivity (9 mS/m) was injected just below the bottom of the logged zone, which was 10 to 15 m above the bottom of the well. The total volume of water injected during recirculation was 1.5 to 4 times the borehole volume. By the end of the recirculation periods the electric conductivity of the pumped water had stabilized at less than 60 mS/m in the shallow zone and 100 mS/m in the deep zone. During both recirculation and logging periods, water was pumped out of the well with a submersible pump located between 20 and 80 m below the ground surface.

Figure 4 shows the caliper log for Well HDB-11. Over the depth interval of the shallow zone (Koetoi Formation, 150 – 450 mbgs) the wellbore diameter is nearly constant at 164 mm. Over the depth interval of the deep zone (Wakkanai Formation, 450 – 800 mbgs) the wellbore diameter is more variable: Below 550 m depth, it is nearly constant at 162 mm, but above 550 m it gradually increases to 240 mm. This diameter increase will cause peaks in FFEC profiles to move upward more slowly. Thus, if the change in borehole diameter is not accounted for, data analysis will result in feed-point strengths that are underestimated over the depth interval 450 – 550 m.

FFEC logging was repeated three times for both the shallow and deep zones, using different pumping rates. **Table 1** shows the schedule of tests. For the shallow zone logging was conducted using pumping rates of 2 L/min, 10 L/min, and 19.1 L/min. **Figure 5** shows the resulting FFEC profiles and **Figure 6** shows water level versus time for each test. For the deep zone, logging was conducted using pumping rates of 5 L/min,

298 10 L/min, and 15 L/min. **Figure 7** shows the resulting FFEC profiles and **Figure 8**
299 shows water level versus time for each test.
300
301 Visual examination of the FFEC profiles (**Figure 5 and Figure 7**) indicates that not
302 all the profiles can be used for analysis. In some cases it appears that the tool that
303 measures fluid electric conductivity did not function at all (e.g., **Figure 5**, Q = 19.1
304 L/min, 5 hr profile). In other cases, the results look qualitatively correct, but the profiles
305 appear shifted with depth or otherwise distorted (e.g., **Figure 7**, Q = 5 L/min, 4 hr and 5
306 hr profiles), suggesting that the tool did not move freely through the wellbore.
307 Subsequent analysis suggests that the problems were caused by slime (muddy water used
308 in drilling) adhering to the sensor. A total of 7 FFEC profiles obtained during the six
309 tests were not included in the analysis because the FFEC profiles were not internally
310 consistent with the remainder of the profiles; they are identified as "unusable FFEC
311 profile" in **Table 1**.
312
313 Water-level data (**Figure 6 and Figure 8**) was collected during the FFEC logging.
314 For the shallow-zone tests, pumping rate increased by an unknown amount for a short
315 period of time early in the tests, then returned to its specified value (**Table 1**). The water
316 level in the wellbore dropped sharply during the high pumping-rate period, then declined
317 at a nearly linear rate in response to the constant pumping rate (**Figure 6**). For the deep-
318 zone tests, water-level data also shows a sharp early drop during the first few minutes of
319 the test, followed by a more gradual decline (**Figure 8).** The gradual decline of the deep-
320 zone tests is less linear than for the shallow-zone tests, showing a decreasing rate of
321 water-level change. The times at which FFEC logs were collected are also shown on
322 **Figure 6** and **Figure 8**.
323
324 We assume that pumping rate Q is the sum of two terms, Q_{wb} and Q_{form}, where Q_{wb} is
325 water that is removed from the wellbore as the water-level in the well declines and Q_{form}
326 is water that comes out of the formation. Q_{wb} can be estimated by multiplying the rate at
327 which water level declines by the cross-sectional area of the wellbore at the depth of the
328 water table. A linear decline in water level corresponds to a constant value of Q_{wb}, and

coupled with a constant value of Q, results in a constant value of Q_{form}, which greatly simplifies the BORE II analysis. Therefore, no logs collected during the initial period of high pumping rate are used for the BORE II analysis. Moreover, for the shallow-zone tests, Q_{wb} is reasonably constant, suggesting that treating Q_{form} as a constant will be a reasonable assumption. However, for the deep-zone tests, Q_{wb} appears to decrease with time, thus only the logs collected while the water level decline is approximately linear are analyzed. The FFEC logs that are not analyzed because Q_{form} cannot be assumed to be constant are identified in **Table 1**. **Table 2** summarizes the Q, Q_{wb}, and Q_{form} values assumed for the tests, with Q_{wb} determined from the slope of the linear fits to water level versus time data shown in **Figure 6** and **Figure 8**.

Ideally, one would use the water level data obtained during logging (**Figure 6** and **Figure 8**) as an open-hole well test to determine T_{tot}, the transmissivity of the entire interval of the borehole being logged, as described above in Section 2.2. This cannot be done in the present case because we do not know either the entire pumping rate history during the logging period, due to the early-time unknown increase in pumping rate, or the complete drawdown record, due to the slow hydrologic response time of the system.

The presence of drilling mud in the wellbore may impact fluid logging two ways: through its salinity and its density. Possible salinity effects are described in Section 4 below. Density effects are neglected, because although the drilling mud itself is presumably significantly denser than formation fluid, most of the mud should be flushed out of the wellbore during the initial recirculation period.

In Well HDB-11, the borehole temperature varies from 11 to 27^{o}C over the depth range of FFEC logging. Prior to analyzing the FFEC logs with BORE II, the FEC values obtained in the field are temperature-corrected using the relationship (Schlumberger, 1984) $FEC(20^{o}C) = FEC(T)/[1 + S(T - 20^{o}C)]$, with $S = 0.024\ ^{o}C^{-1}$. This correction is required because BORE II assumes a constant temperature of 20^{o}C.

4. Analysis of Shallow FFEC Logs

The numerical model BORE II (Doughty and Tsang, 2000) is used to analyze the three sets of shallow-zone FFEC logs for three pumping rates Q = 2 L/min, 10 L/min, and 19.1 L/min, to obtain a set of inflow locations z_i, feed-point strengths q_i, and salinities C_i. The z_i values are obtained by looking at early-time FFEC profiles, before individual peaks begin to interfere with each other, making z_i easy to determine with good accuracy. Given the inflow locations z_i, the matching process is then conducted with salinities C_i adjustable but maintained the same for all three data sets, while the feed-point strengths q_i are allowed to be different between the three data sets. Thus, different combinations of q_i and C_i are input to BORE II by trial and error, in order to match the FFEC logs obtained in the field. The matching makes use of the following facts: the area under an isolated FEC peak is proportional to the product q_iC_i, the speed of a peak moving up the wellbore depends only on the sum of q_i values for the current and deeper peaks, and the steady-state height of the deepest peak depends only on C_i. Initial trials consider the C_i to be the same for all inflow points (corresponding to 1,000 mS/m), but this restriction is relaxed as needed to improve the match. At the early stages of the fitting process, each test is treated individually. Later, the q_i values for all three tests are varied concurrently, using Equations (1) and (6) to constrain possible values of $q_i^{(1)}$, $q_i^{(2)}$, and $q_i^{(3)}$ so that the three pairs of tests produce consistent results for T_i/T_{tot} and $I\Delta P_i$.

Figure 9 and **Figure 10** show the best model fit to the subset of FFEC profiles that are amenable to analysis, as listed in **Table 1**. The first profile shown for each test is used as the model initial condition, and as shown in **Table 1**, this is the first profile collected after Q becomes constant. The deepest peak, barely visible at 438 m depth, is not analyzed, as it does not evolve like a peak caused by a normal inflow point. It may be caused by the drilling sludge at the bottom of the wellbore. The next three distinct peaks (depths of 350, 280, and 220 m) show classic growing and skewing behavior. Within a given test (e.g., **Figure 10**, top frame), upward flow within the borehole ("upflow") increases as one moves up the borehole, so peak skewing increases, with the upgradient (deeper) limb of the peak becoming steeper and the downgradient (shallower) limb of the peak becoming flatter. Comparing tests with successively greater pumping

391 rates (e.g., **Figure 10**, all three frames, peak at 280 m) shows the same pattern: as
392 pumping rate increases, upflow increases and peak skewing increases. The model
393 matches for all these peaks are very good and the distinctive dependence of peak features
394 on upflow means that the corresponding estimates for feed-point strengths are well
395 constrained.
396
397 Another unknown parameter that is determined by trial and error along with the q_i
398 and C_i values is the solute dispersion coefficient in the borehole. Because the FEC probe
399 is moving up and down the well, and the well is being pumped, this dispersion coefficient
400 is generally several orders of magnitude bigger than the molecular diffusion coefficient.
401 We obtain a value of 0.004 m^2/s for the dispersion coefficient.
402
403 The largest, shallowest peak at 164 m shows very little upflow (**Figure 9**), in fact
404 significantly less than the upflow shown by the smaller deeper peaks. The upgradient
405 limb of this peak is steep, consistent with the upflow inferred by matching the deeper
406 peaks. However, the downgradient limb of this peak is not as flat as would be expected
407 for continued upflow. This suggests that there is either an outflow just above the large,
408 shallow peak, or an inflow of low-salinity water there. One possibility is that low-salinity
409 shallow groundwater got into fractures at this level during the recirculation operation, and
410 is moving back into the wellbore during logging. This situation is too complicated to
411 model with any accuracy, so the large shallow peak is not included in the quantitative
412 analysis, but we can infer from this behavior that its transmissivity is large and the far-
413 field pressure head is low at this depth.
414
415 An interesting observation from the FFEC logs that has not been seen in previous
416 studies involving granitic rock (Doughty et al., 2005) is that the FEC value grows
417 uniformly in time where discrete peaks are not present (e.g., around 375 m depth in
418 **Figure 10**). We hypothesize that the wellbore walls have been coated with drilling mud,
419 which contains salt that diffuses into the wellbore fluid, causing a small FEC increase all
420 along the borehole interval. To simulate this effect we introduce numerous tiny feed
421 points distributed uniformly along the wellbore, with the same q_iC_i, which is then varies

to match the portion of FFEC profiles where no discrete peaks exist. These tiny feed points are designed to have q_i small enough to have a negligible effect on flow up the wellbore. Including these extra feed points results in a slightly improved match to the shallow FFEC profiles, but the derived parameters q_i and C_i for the peaks are not significantly changed. In conclusion, for this particular data set, the discrete FEC peaks are large enough so that the diffusion effect is negligible.

The direct-fit results of for the shallow-zone tests are shown in **Figure 11.** Note that the C_i values are presented as equivalent FEC value, with units of mS/m, and that the values of z_i and C_i are the same for the three tests; only the q_i values are allowed to be different between the three tests. Comparison of the C_i values with salinity and electric resistivity values found in other HDB Wells in the area (Yamamoto et al., 2002a, 2002b) shows that the values of C_i obtained by FFEC logging are consistent with those obtained by independent measurements.

The mass integral, or $M(t)$ method, provides a way to look at the overall behavior of all the fractures intersecting the wellbore at one time, and can provide useful information for helping the FFEC log fitting process. In the $M(t)$ method, we integrate each $C(z)$ profile over the wellbore section of interest to obtain the area $A(t)$ under the $C(z)$ profile at time t. Then, we multiply $A(t)$ by the mean wellbore cross-sectional area to determine ion mass in place at time t, which we denote as the mass integral $M(t)$, and plot $M(t)$ versus t (for the present study, with C represented in equivalent units of FEC, $M(t)$ is not a true mass, but the principle remains the same). If peaks reach the upper limit of the integration, a correction factor is introduced to account for mass being lost from the system, enabling subsections of the logged interval to be examined. **Figure 12** shows a schematic diagram of three $M(t)$ integrals for the depth interval between 500 and 775 m.

If q_i and C_i do not vary in time for any feed points; and additionally if all feed points are inflow points, $M(t)$ will be linear. Thus, deviations of $M(t)$ from linearity provide information on the validity of model assumptions. If $M(t)$ is concave up, it indicates that either q_i increases in time (a transient response to pumping) and/or that C_i increases in

time (low-salinity shallow groundwater moved into fractures during recirculation so that during pumping inflow begins with low C_i values and increases to formation-water value). In contrast, if $M(t)$ is concave down, it suggests that q_i decreases in time or that outflow points are present.

Figure 13 show the $M(t)$ versus t plots for the shallow-zone logs between depths of 180 and 440 m (i.e., the largest, shallowest peak at 164 m is excluded). For each test, $M(t)$ is slightly concave up at early times, which we interpret as representing the early-time production of low-salinity shallow groundwater that had moved into the fractures during recirculation. The model is able to reproduce this behavior, despite assuming constant C_i values, by employing a starting time $t_{0i} > 0$ at which each feed-point begins to have a non-zero value of C_i. The t_0 values shown in **Figure 13** are averages over the t_0 values for individual feed points. In order to obtain more accurate results from the fitting process, we focus on FFEC profiles collected during the period when $M(t)$ is linear. Generally, the agreement between the model and field values of $M(t)$ is very good, providing additional confidence in the fitting method.

Results of the multi-rate analysis are shown in **Figure 14** and **Table 3**. A total of 26 feed points are identified between depths of 180 and 420 m. **Figure 14** shows that there is good consistency between T_i/T_{tot} and $I\Delta P_i$ values obtained using results of three different pairs of tests. Coupled with the good matches to the FFEC profiles themselves (**Figure 10**), and the fact that the feed-point salinities are all within the range shown for other HDB wells in the area (Yamamoto et al., 2002a, 2002b), this consistency provides a measure of confidence in the correctness of the FFEC analysis results.

5. Analysis of Deep FFEC Logs

Because the water-level data for the deep-zone tests (**Figure 8**) is not as linear as one would like, the $M(t)$ analysis was done for the deep-zone tests prior to direct fitting, to provide guidance on which profiles may be most amenable to analysis. Results are shown in **Figure 15**. All $M(t)$ profiles are concave up at early times, suggesting that,

consistent with the water-level data, Q_{wb} is decreasing in time and Q_{form} is increasing. Additionally, there is the possibility that $C_i(t)$ is affected by low-salinity shallow groundwater that moved into the fractures during recirculation. Thus, the late-time data, when $M(t)$ is more linear, is emphasized in the fitting process. The FFEC profile used for model initial conditions (**Figure 15**) is not the first one available, but a later profile chosen so that the model period will correspond more closely to the time period when $M(t)$ is linear.

Matching the FFEC profiles for the deep-zone logs followed the same procedure as for the shallow-zone logs (described in the first paragraph of Section 4). Initially the matching process assumed that all feed points had the same salinity (corresponding to 3000 mS/m). During the matching process, variable C_i values were introduced as needed to improve the match. For the dispersion coefficient, a value of 0.005 m^2/s was obtained, nearly the same as for the shallow zone.

The FFEC profiles used for the analysis and the best model fit are shown in **Figure 16**. The match is excellent for the peaks below 620 m. The match for the large peaks at 603 m and 611 m is not quite as good, and this error propagates upward, making the matches for peaks above 600 m somewhat worse as well. Direct-fitting results of the individual tests are shown in **Figure 17**. Multi-rate results are shown in **Figure 18** and **Table 4**. A total of 18 deep feed points are identified.

Results for depths above 540 m less certain because of the wellbore diameter change. It is interesting to note from **Table 2** that the sum of the feed-point strengths Σq_i is less than the value hypothesized for Q_{form}. This could be partly attributable to the diameter change, but rough calculations suggest that the effect is not big enough to account for the whole discrepancy. A bigger issue is the uncertainty in Q_{form} itself, due to the variation of Q_{wb}.

6. Comparison with Packer-Test Results

During the surface-based investigations (Phase 1) of the Horonobe URL project, conducted between years 2000 and 2005, a total of 11 deep boreholes (HDB-1 through HDB-11) were drilled for an underground investigation of the geological environment in and around the main URL area at Horonobe. Well HDB-11, the deepest borehole (1,020 m) in the URL area, was drilled during 2005 and 2006 (**Figure 3**). A sequential approach to hydraulic testing was employed at Well HDB-11, in which packer inflation, shut-in, pressure recovery, pulse test, slug test, long-term pumping test, and packer deflation were sequentially conducted in each of 10 packed-off intervals. The transient pressure responses to the multiple testing events in each interval were measured. In order to calculate hydraulic parameters such as transmissivity, hydraulic conductivity, storativity, and specific storage for each interval, standard analysis methods assuming radial flow geometry, such as those of Cooper, Agarwal, Hvorslev and Jacob, are applied to the pressure-transient data. Then the best fit parameters are selected as the representative values. **Table 5** summarizes the depths of the packed-off intervals, estimated hydraulic parameters, static pressure heads in the packed-off intervals, testing events, and the analysis methods applied to obtain hydraulic parameters, for the successful tests.

Packer test results were made available to us after the conclusion of our FFEC analyses. They provide transmissivity and far-field hydraulic head values for seven 10-80 m intervals along the borehole where FFEC logging was done (**Figure 19**). In order to compare FFEC analysis results for the normalized transmissivity of fracture *i*, T_i/T_{tot}, to packer test results for transmissivity of interval L, $T_{L\text{-}pt}$, individual values of T_i/T_{tot} are summed over the depth intervals of the packer tests to obtain $T_{L\text{-}fec}$. Recall that transmissivity T (m^2/s) is an extrinsic property – it is proportional to the product of intrinsic permeability and a thickness – so simply summing over T_i produces T_L, and there is no need to weigh different T_i values by fracture aperture or be concerned with fracture spacing. For the Lth interval

$$T_{L-fec} = \sum_{i \subset L} T_i = T_{tot} \sum_{i \subset L} \left(\frac{T_i}{T_{tot}} \right). \qquad (7)$$

The introduction of T_{tot} on far right-hand-side is required because FFEC analysis just provides the ratio of transmissivities (T_i/T_{tot}), not the absolute transmissivity value T_i. Recall that T_{tot} is the total transmissivity of the borehole interval that is open during logging. In the present case, we do not have any independent measurements to provide T_{tot}, so it is chosen by hand, as the value which produces the best overall match between all the $T_{L\text{-}fec}$ and $T_{L\text{-}pt}$ values within each zone. This resulting values of T_{tot} for the shallow and deep zones are presented in **Table 6**.

The average far-field hydraulic head of interval L is denoted P_L. The value measured by the packer tests is denoted $P_{L\text{-}pt}$. The value determined by FFEC logging is denoted $P_{L\text{-}fec}$, and is obtained by averaging over far-field head values of individual fractures P_i

$$P_{L-fec} = \frac{\sum_{i \subset L} P_i T_i}{T_{L-fec}}. \tag{8}$$

However, because the multi-rate FFEC logging method does not determine the P_i values directly, but rather the ratio given by Equation (2), Equation (8) does not provide a simple means for determining $P_{L\text{-}fec}$. Therefore, we proceed first by rearranging Equation (6) to provide an expression for P_i in terms of the outputs of a multi-rate FFEC analysis and the productivity index I

$$P_i = P_{avg} + \frac{Q_1}{I}\left(\frac{q_i^{(1)}/Q_1}{T_i/T_{tot}} - 1 \right). \tag{9}$$

Then, simple algebra may be used to produce the comparable expression for $P_{L\text{-}fec}$:

$$P_{L-fec} = P_{avg} + \frac{Q_1}{I}\left(\frac{\sum_{i \subset L} q_i^{(1)}/Q_1}{T_{L-fec}/T_{tot}} - 1 \right). \tag{10}$$

Recall that I is defined as the ratio of pumping rate to drawdown for an open-borehole well test

$$I = \frac{Q}{P_{avg} - P_{wb}}. \tag{11}$$

For the present analysis, no independent well test was done, so the value of I is determined from water-level data collected during FFEC logging (**Figure 6** and **Figure**

566 **8**). For the deep zone, reasonably consistent values of I are obtained for the three tests,
567 using the late-time pressure differences and the sum of the model values of q_i in place of
568 Q (since the reported pumping rate is found not to represent the flow coming from the
569 formation and therefore cannot be used to determine I).
570
571 For the shallow zone, the large shallowest peak complicates matters so that a single
572 consistent value of I cannot be obtained for the three tests. To determine an appropriate
573 value of I to use for the shallow-zone analysis, we assume that radial flow geometry
574 applies for all feed points and combine Equations (4) and (11) to yield

575 $$\frac{T_{tot}}{I} = 2\pi \ln\left(\frac{r_i}{r_{wb}}\right). \qquad (12)$$

576 Our conceptual model is that all intervals have the same radial flow geometry, so it is
577 reasonable to further assume that the shallow and deep intervals also have similar flow
578 geometries, that is, similar values of r_i. Since r_i appears within a logarithm, T_{tot}/I is not
579 very sensitive to r_i.. Then, given T_{tot} for the shallow and deep zones from Equation (7), I
580 for the shallow zone can be determined from Equation (12) using the value of r_i
581 determined for the deep zone. I and r_i values determined in this manner are given in
582 **Table 6**.
583
584 Equation (10) indicates that the value of I controls the spread among $P_{L\text{-}fec}$ values for
585 different intervals and that P_{avg} simply provides a constant shift to the different $P_{L\text{-}fec}$
586 values. P_{avg} appears in the derivation because the multi-rate analysis just determines the
587 relative values of P_i, and not their absolute values. P_{avg} is determined by hand as the
588 value which produces the best overall match between all the $P_{L\text{-}fec}$ and $P_{L\text{-}pt}$ values within
589 each zone. The resulting values of P_{avg} for the shallow and deep zones are shown in
590 **Table 6**.
591
592 **Figure 19** compares the transmissivities and pressure heads obtained from the packer
593 tests with the results of the multi-rate analysis. Note that the deep logged interval extends
594 to 775 m in depth, but no peaks develop below 700 m. This is consistent with the very
595 low transmissivity obtained for the packer-test interval from 700-730 m. Generally, the

FEC-derived values show more variability between intervals than do the packer-test values, for both transmissivity and pressure head. However, for most intervals the observed trends between values are the same for both methods (e.g., for the deep zone, the shallowest interval has a much higher head value than do the three deeper intervals).

7. Discussion

In a system with a rapid hydrologic response, the water level in the borehole would drop quickly in response to the onset of pumping, and remain at a steady value thereafter. Thus after a short transient period, Q_{wb} would be zero and Q_{form} would equal the pumping rate Q, a constant, and the steady-flow assumption of BORE II would be met. We would use the difference between the unpumped water level P_{avg} and the pumped water level P_{wb} as part of the multi-rate analysis.

The non-steady water level observed during logging in the present set of measurements (**Figure 6** and **Figure 8**) indicates that the hydrologic response of the system to the initiation of pumping is quite slow, and in fact water level changes throughout the logging period. This complicates several facets of the FFEC analysis. At a fundamental level, the assumption of steady-state flow from the formation to the wellbore, Q_{form}, which BORE II relies on, may not be valid at all times. We can use water-level data and $M(t)$ analysis to ascertain which portions of the logging period have a constant Q_{form}: for a constant pumping rate Q, a linearly declining water level implies a constant Q_{wb} and hence a constant Q_{form}, and a linear $M(t)$ implies a constant Q_{form} and constant C_i values.

Moreover, with a slowly responding system, it is difficult to determine P_{wb}, and even difficult to ascertain whether the pressure measured before pumping begins is truly representative of P_{avg}. With Q_{form} uncertain, the possibility to constrain the q_i with the relationship $\Sigma q_i = Q_{form}$ diminishes. An open-hole well test to determine T_{tot}, natural-state pressure head P_{avg}, and drawdown $P_{avg} - P_{wb}$ would remove some uncertainty. Such results would also be useful for comparing to FFEC results and to packer-test results.

Generally, the shallow-zone tests show more linear water-level declines than do the deep-zone tests, enabling Q_{form} to be ascertained, but the complicated nature of the shallow peak at 164 m depth precludes a complete analysis in which $\Sigma q_i = Q_{form}$ can be demonstrated. It is fortuitous that the peak that cannot be analyzed is the shallowest peak, because as such it has no affect on any deeper peaks. Generally, any peaks occurring above a non-analyzable peak would also be non-analyzable. For the deep-zone tests, all the peaks can be analyzed, but the non-linearity of the water-level decline suggests that Q_{form} is not constant, again precluding the constraint $\Sigma q_i = Q_{form}$ from being used.

During the deep-zone matching procedure, it became apparent that the FFEC profiles could be equally well matched with alternative sets of salinity values. This non-uniqueness points out the usefulness of independent information when applying the FFEC method. **Figure 20** compares the electric conductivity obtained from groundwater squeezed from core samples obtained during the drilling of Well HDB-11 with the FEC_i values inferred from FFEC logging. Of course, there is not expected to be a one-to-one correspondence between the two independently-obtained data sets, as core samples mainly contain groundwater held in the rock matrix, as opposed to FFEC analysis results, which are on groundwater moving through fractures. Because matrix permeability is much smaller than fracture permeability, the spatial range that the conductivity values represent is quite different, and it is thus reasonable that they differ somewhat. However, the general consistency between the two data sets shown in **Figure 20** lends credence to the FFEC results.

8. Conclusions

In spite of the various complications associated with the test data described in the analysis sections above, the three days of FFEC logging for the shallow zone have yielded internally consistent information on location, salinity, and transmissivity and

656 inherent "steady-state" pressure heads of 26 conducting fractures, over depths from 150
657 to 450 m (Table 3). Also, three days of FFEC logging for the deep zone yielded the same
658 information for 18 conducting fractures over depths from 450 to 775 m.
659
660 A careful study was made to compare the detailed results on these 44 conducting
661 fractures with transmissivity and hydraulic data of seven packed-off intervals with
662 interval length ranging from 10 to 80 m. Overall, it has been shown that the FFEC
663 logging results are consistent with these independent data. Generally, the individual
664 fracture hydraulic properties obtained from FFEC logs yield more variability between
665 intervals than do the packer tests. However, for the most part, the observed trends
666 between different intervals are the same for both methods. The success of the FFEC
667 analysis method under these complicated conditions provides evidence of the robustness
668 of the method.
669
670 Below we give some remarks concerning possible further FFEC log analysis to
671 improve confidence in FFEC logging results, and also a number of recommendations for
672 improving the field procedure for future FFEC logging applications.
673
674 For the shallow-zone tests, we get a good match for all the small peaks. Only the
675 uppermost, largest peak is not analyzable. Without this peak it is impossible to verify
676 whether or not $\Sigma q_i = Q_{form}$. For the deep-zone tests, we get a reasonably good match for
677 all the peaks, but the fact that $\Sigma q_i < Q_{form}$ is problematic. It could simply be a
678 consequence of the non-linear borehole water-level decline that identifies Q_{form} is an
679 increasing function of time, or it could indicate that inflow to the well occurs above the
680 depth interval that was logged.
681
682 A number of further analyses are possible, in order to improve our confidence in the
683 results. We could specify time-dependent feed-point strengths q_i(t), to account for a
684 time-dependent Q_{form}, and time-dependent feed-point salinities C_i(t), to account for the
685 presence of low-salinity shallow groundwater water in the fractures at the onset of
686 pumping. We could also model the recirculation period and the rest period between the

end of the recirculation period and the onset of pumping, in order to develop more accurate initial conditions for the logging period.

For the deep-zone tests, we could try to account for the variable wellbore diameter. It may be possible to do this with fictitious outflow points as was done in Doughty et al. (2005) for a simple one-time change in borehole diameter. Another alternative would be to modify the BORE II code itself to enable variable borehole diameters to be considered.

Concerning potential improvements of field test procedures for future FFEC logging applications, we make the following recommendations:

1. If possible, do recirculation at a lower rate, to minimize flow of low-salinity groundwater into fractures.
2. Keep the pumping rate constant during logging, or at least measure rate changes if they are unavoidable.
3. Continue logging until logs show evidence of the approach to steady-state FFEC profiles (plateaus). Plateaus greatly reduce ambiguity in parameter choice for diffusion coefficient, q_i, C_i.
4. Continue logging until water level in the wellbore is constant or linearly declining, to enable Q_{form} to be determined unambiguously.
5. If possible, emplace a packer in the well just above the pump to avoid the problem of a declining water level in the well during pumping (i.e., setting $Q_{wb} = 0$).
6. If a profile of FEC is distorted by muddy water adhering to a sensor, withdraw and clean the sensor and repeat the log.
7. Obtain and use (at least) one salinity measurement at a deeper borehole inflow point in FFEC log analysis. This can greatly reduce the non-uniqueness inherent in matching peaks that do not move strongly up the well.

Acknowledgments

We thank Kenzi Karasaki of Lawrence Berkeley National Laboratory for his careful review of this paper. This work was supported by the Japan Atomic Energy Agency

(JAEA) under the Binational Research Cooperative Program between JAEA and the U.S. Department of Energy, Office of Civilian Radioactive Waste Management, Office of Science and Technology. The work was performed under the auspices of the U.S. Department of Energy through Contract No. DE-AC02-05CH1123.

References

Bauer, G.D. and J.J. LoCoco, Hydrogeophysics determines aquifer characteristics, International Ground Water Technology, 12-16, August/September, 1996.

Brainerd, R.J. and G.A. Robbins, A tracer dilution method for fracture characterization in bedrock wells, Ground Water, 42(5), 774-780, 2004.

Doughty, C. and C.-F. Tsang, BORE II – A code to compute dynamic wellbore electrical conductivity logs with multiple inflow/outflow points including the effects of horizontal flow across the well, Rep. LBL-46833, Lawrence Berkeley National Laboratory, Berkeley, CA, 2000.

Doughty, C. and C.-F. Tsang, Signatures in flowing fluid electric conductivity logs, J. of Hydrology, 310, 157-180, 2005.

Doughty, C., S. Takeuchi, K. Amano, M. Shimo and C.-F. Tsang. Application of Multi-rate Flowing Fluid Electric Conductivity Logging Method to Well DH-2, Tono Site, Japan, Water Resources Res, 41, W10401, doi:10.1029/2004WR003708, 2005.

Drost, W., D. Klotz, A. Koch, H. Moser, F. Neumaier, and W. Rauert, Point dilution methods of investigating ground water flow by means of radioisotopes, Water Resour. Res., 4(1), 125-146, 1968.

Evans, D.G., Inverting fluid conductivity logs for fracture inflow parameters, Water Resour. Res., 31(12), 2905-2915, 1995.

Evans, D.G., W.P. Anderson, Jr., and C.-F. Tsang, Borehole fluid experiments near salt contamination sites in Maine, in proceedings of the NGWA Conference on Eastern Regional Ground Water Issues, Boston, 797-807, 1992.

Hale, F.V. and C.-F. Tsang, A code to compute borehole conductivity profiles from multiple feed points, Rep. LBL-24928, Lawrence Berkeley Laboratory, Berkeley, CA, 1988.

Hale, F.V. and C.-F. Tsang, VHBORE: A code to compute borehole fluid conductivity profiles with pressure changes in the borehole, Rep. LBL-31050, Lawrence Berkeley Laboratory, Berkeley, CA, 1994.

759
760 Guyonnet, D., A. Rivera, S. Löw and N. Correa, Analysis and synthesis of fluid logging
761 data from Wellenberg boreholes SB1, SB3, SB4 and SB6, Nagra Tech. Rep. NTB 92-01,
762 pp. 153, Nagra, Wettington, Switzerland, 1993.
763
764 Karasaki, K., B. Freifeld, A. Cohen, K. Grossenbacher, P. Cook, and D. Vasco, A
765 multidisciplinary fractured rock characterization study at Raymond field site, Raymond,
766 CA, J. of Hydrology, 236, 17-34, 2000.
767
768 Kelley, V. A., J. M. Lavanchy, and S. Löw, Transmissivities and heads derived from
769 detailed analysis of Siblingen 1989 fluid logging data, Nagra Tech. Rep. NTB 90-09, pp.
770 184, Nagra, Wettington, Switzerland, 1991.
771
772 Löw, S., V. Kelley, and S. Vomvoris, Hydraulic borehole characterization through the
773 application of moment methods to fluid conductivity logs, J. App. Geophys., (31(1-4),
774 117-131, 1994.
775
776 Marschall, P. and S. Vomvoris (editors), Grimsel Test Site: Developments in
777 hydrotesting, fluid logging and combined salt/heat tracer experiments in the BK Site
778 (Phase III), Nagra Tech. Rep. 93-47, Nagra, Wettingen, Switzerland, 1995.
779
780 Öhberg, A. and P. Rouhiainen, Groundwater flow measuring techniques, Posiva 2000-12,
781 Posiva Oy, Helsinki, Finland, 2000.
782
783 Paillet, F.L. and W.H. Pedler, Integrated borehole logging methods for wellhead
784 protection applications, Engineering Geology, 42(2-3), 155-165, 1996.
785
786 Pedler, W.H., C.L. Head, and L.L. Williams, Hydrophysical logging: A new wellbore
787 technology for hydrogeologic and contaminant characterization of aquifers, National
788 Outdoor Action Conference, National Ground Water Association, Las Vegas, Nevada,
789 1992.
790
791 Schlumberger, Ltd., Log interpretation charts, New York, 1984.
792
793 Tsang, C.-F. and C. Doughty, Multi-Rate Flowing Fluid Electric Conductivity Method,
794 Water Resources Res, 39(12), pp. 1354-1362, 2003.
795
796 Tsang, C.-F., P. Hufschmied, and F.V. Hale, Determination of fracture inflow parameters
797 with a borehole fluid conductivity logging method, Water Resources Res., 26(4), pp. 561-
798 578, 1990.
799
800 Yamamoto, T., M .Shimo, Y. Fujiwara, H. Hattori, T. Tadokoro, H. Iwama, M. Nago,
801 and S. Kumamoto, HDB-1 borehole investigations in Horonobe Underground Research
802 Center, Japan Atomic Energy Agency Report JNC TJ1400 2002-010 (in Japanese),
803 2002a.
804

Yamamoto, T., M .Shimo, Y. Fujiwara, H. Hattori, T. Tadokoro, H. Iwama, M. Nago, and S. Kumamoto, HDB-2 borehole investigations in Horonobe Underground Research Center, Japan Atomic Energy Agency Report JNC TJ1400 2002-011 (in Japanese), 2002b.

Tables

Table 1-1. Operation table for shallow-zone Test 1, pumping rate 2 L/min; Date Nov 30-Dec 1, 2004; logging interval 147-440 mbgs (I.C. = initial-condition profile)

Event	Time (hr:min)	Cable speed (m/min)	Comments
Recirculation of low-salinity groundwater	15:25 – 19:05		23,000 L
FFEC log, no pumping	21:56 – 22:11	19.5	
Start pump	23:00		
FFEC log, 0 hour later	23:05 – 23:20	19.5	Skip, variable Q_{form}
High pump rate	23:58 – 0:08		
FFEC log, 1 hour later	0:05 – 0:20	19.5	Use as I.C.
FFEC log, 2 hours later	1:05 – 1:20	19.5	
FFEC log, 3 hours later	2:05 – 2:20	19.5	
FFEC log, 4 hours later	3:05 – 3:20	19.5	
FFEC log, 5 hours later	4:05 – 4:20	19.5	
FFEC log, 6 hours later	5:05 – 5:20	19.5	
Stop pump	16:28		

Table 1-2. Operation table for shallow-zone Test 2, pumping rate 10 L/min; Date Dec 1, 2004; logging interval 147-440 mbgs (I.C. = initial-condition profile)

Event	Time (hr:min)	Cable speed (m/min)	Comments
Recirculation of low-salinity groundwater			12,000 L
FFEC log, no pumping	14:55 – 15:10	19.5	
Start pump	15:53		
High pump rate	15:53 – 16:05		
FFEC log, 0 hour later	16:05 – 16:20	19.5	Use as I.C.
FFEC log, 1hour later	17:05 – 17:20	19.5	
FFEC log, 2 hours later	18:05 – 18:20	19.5	
FFEC log, 3 hours later	19:05 – 19:20	19.5	
FFEC log, 4hours later	20:05 – 20:20	19.5	
FFEC log, 5 hours later	21:05 – 21:20	19.5	
FFEC log, 6 hours later	22:05 – 22:20	19.5	
Stop pump	22:39		

817 Table 1-3. Operation table for shallow-zone Test 3, pumping rate 19.1 L/min; Date Dec
818 2, 2004; logging interval 147-440 mbgs (I.C. = initial-condition profile)

Event	Time (hr:min)	Cable speed (m/min)	Comments
Recirculation of low-salinity groundwater	10:58 – 13:36		33,000 L
FFEC log, no pumping	16:03 – 16:18	19.5	
Start pump	17:34		
High pump rate	17:34 – 17:54		
FFEC log, 0 hour later	17:55 – 18:10	19.5	Use as I.C.
FFEC log, 1 hour later	18:55 – 19:10	19.5	
FFEC log, 2 hours later	19:55 – 20:10	19.5	
FFEC log, 3 hours later	20:55 – 21:10	19.5	
FFEC log, 4 hours later	21:55 – 22:10	19.5	
FFEC log, 5 hours later	22:55 – 23:10	19.5	Unusable FFEC profile
Stop pump	23:25		

819
820 Table 1-4. Operation table for deep-zone Test 1, pumping rate 5 L/min; Date Jan 30,
821 2005; logging interval 442-780 mbgs (I.C. = initial-condition profile)

Event	Tme (hr:min)	Cable speed (m/min)	Comments
Recirculation of low-salinity groundwater	17:30 – 5:00		42,000 L
FFEC log, no pumping	8:23-8:39	21.1	
Start pump	9:32		
FFEC log, 0hour later	9:45 – 10:00	22.5	Skip, variable Q_{form}
FFEC log, 1hour later	10:45 – 11:02	19.9	Use as I.C.
FFEC log, 2hours later	11:45 – 12:01	21.1	
FFEC log, 3hours later	12:45 – 13:00	22.5	
FFEC log, 4hours later	13:45 – 14:00	22.5	Unusable FFEC profile
FFEC log, 5hours later	14:50 – 15:07	19.9	Unusable FFEC profile
FFEC log, 6hours later	16:03 – 16:19	21.1	
Stop pump	16:28		

822
823

Table 1-5. Operation table for deep-zone Test 2, pumping rate 10 L/min; Date Jan 31, 2005; logging interval 442-775 mbgs (I.C. = initial-condition profile)

Event	Time (hr:min)	Cable speed (m/min)	Comments
Recirculation of low-salinity groundwater	19:30 – 6:30		38,000 L
FFEC log, no pumping	8:05 – 8:23	18.5	
Start pump	9:11		
FFEC log, 0hour later	9:25 – 9:42	19.6	Skip, variable Q_{form}
FFEC log, 1hour later	10:25 – 10:42	19.6	Unusable FFEC profile
FFEC log, 2hours later	11:25 – 11:43	18.5	Use as I.C.
FFEC log, 3hours later	12:25 – 12:42	19.6	
FFEC log, 4hours later	13:25 – 13:43	18.5	
FFEC log, 5hours later	14:25 – 14:42	19.6	
FFEC log, 6hours later	15:25 – 15:43	18.5	
FFEC log, 7hours later	16:25 – 16:42	19.6	
Stop pump	16:58		

Table 1-6. Operation table for deep-zone Test 3, pumping rate 15 L/min; Date Feb 1, 2005; logging interval 440-772 mbgs (I.C. = initial-condition profile)

Event	Time (hr:min)	Cable speed (m/min)	Comments
Recirculation of low-salinity groundwater	19:30 – 6:20		39,000 L
FFEC log, no pumping	8:05 – 8:22	19.5	
Start pump	9:30		
FFEC log, 0hour later	9:40 – 9:56	20.8	Skip, variable Q_{form}
FFEC log, 1hour later	10:40 – 10:57	19.5	Use as I.C.
FFEC log, 2hours later	11:40 – 11:58	18.4	
FFEC log, 3hours later	12:40 – 12:57	19.5	
FFEC log, 4hours later	13:40 – 13:55	22.1	
FFEC log, 5hours later	14:40 —?	—	
FFEC log, 6hours later	15:40 – 15:55	22.1	Unusable FFEC profile
FFEC log, 7hours later	16:40 – 16:57	19.5	Unusable FFEC profile
FFEC log, 8hours later	17:40 – ?	—	Unusable FFEC profile
Stop pump	18:03		

Table 2. Q, Q_{wb}, and Q_{form} for the various tests. In each case $Q_{form} = Q - Q_{wb}$, with Q_{wb} determined from the slope of the linear fits to water level versus time data shown in **Figure 6** and **Figure 8.**

	Q (L/min)	Q_{wb} (L/min)	Q_{form} (L/min)	Σq_i	Comment
Shallow Tests	2	0.69	1.31	1.31	Σq_i unreliable because q of shallowest peak cannot be determined accurately
	10	5.82	4.18	4.18	
	19.1	12.76	6.34	6.34	
Deep Tests	5	1.66	3.34	2.04	Σq_i much less than Q_{form}
	10	3.16	6.84	3.90	
	15	7.15	7.85	5.12	

834
835
836 Table 3. Multi-rate analysis results for shallow-zone tests.

Peak Number	Depth (m)	C_i (mS/m)	T_i/T_{tot}	$I\Delta P_i$
1	417	1000	0.013	-0.338
2	402	1000	0.019	-0.380
3	385	1000	0.005	-0.768
4	370	1000	0.007	-0.816
5	360	1000	0.014	-0.224
6	351	750	0.050	0.268
7	348	750	0.048	0.130
8	338	1000	0.013	0.287
9	332	1000	0.011	0.393
10	325	1000	0.009	-0.403
11	316	1000	0.009	-0.186
12	312	1000	0.013	-0.554
13	299	1000	0.008	0.814
14	292	2000	0.007	1.626
15	287	2000	0.006	0.828
16	282	2000	0.048	0.058
17	278	2000	0.036	0.358
18	262	450	0.086	0.342
19	259	450	0.063	0.306
20	248	1000	0.041	-0.242
21	226	1000	0.221	-0.381
22	220	1000	0.044	0.225
23	219	1000	0.067	-0.076
24	211	1000	0.029	0.283
25	201	1000	0.061	0.668
26	190	1000	0.044	-0.276

837
838

838 Table 4. Multi-rate analysis results for deep-zone tests.

Peak Number	Depth (m)	C_i (mS/m)	T_i/T_{tot}	$I\Delta P_i$
1	674	2200	0.114	0.672
2	656	2000	0.065	-1.438
3	648	2000	0.029	-0.411
4	633	2000	0.030	-0.518
5	629	2000	0.021	-0.371
6	618	15000	0.011	-0.732
7	611	15000	0.384	-0.301
8	603	3000	0.016	1.229
9	591	12500	0.020	1.587
10	575	15000	0.046	2.584
11	566	7000	0.009	3.573
12	544	6000	0.002	-0.332
13	530	6000	0.078	-0.271
14	522	5000	0.036	-0.856
15	484	5000	0.101	-0.227
16	478	5000	0.016	-0.246
17	473	5000	0.016	-0.246
18	463	5000	0.009	-0.292

839

839 Table 5. Summary of packer-test results.

Packed-off intervals			Stratigraphy	FFEC Logging Zone	Test results (representative values)		
Upper end (mbgl)	Lower end (mbgl)	Interval thickness (m)			Transmissivity (m^2/sec)	Static head (G.L. m)	Analysis method
55.5	75.5	20	Koetoi F.		2.77E-08	-0.96	Agarwal
115	153	38	Koetoi F.		2.60E-07	-0.07	Cooper
171	237	66	Koetoi F.	shallow	1.37E-07	-0.70	Agarwal
311	380	69	Koetoi F.	shallow	1.40E-07	3.56	Cooper
564	584	20	Wakkanai F.	deep	3.07E-07	5.50	Cooper
606 †	644	38	Wakkanai F.	deep	3.28E-06	5.57	Cooper
606†	644	38	Wakkanai F.	deep	8.63E-07	5.36	Jacob
646	666	20	Wakkanai F.	deep	1.76E-07	5.74	Cooper
670	690	20	Wakkanai F.	deep	2.51E-07	5.08	Cooper
704	724	20	Wakkanai F.	deep	1.25E-10	13.41	Agarwal
923	1000	77	Wakkanai F.		2.01E-08	41.98	Hvorslev

840 † The upper packer-test labeled 606-644 shows the results of a slug test, while the lower
841 606-644 shows results of a long-term pumping test. Therefore, the lower results are more
842 reliable.
843

843 Table 6. Parameters used for comparison between results of multi-rate flowing FFEC
844 logging analysis and packer-tests.

Parameter	Zone	
	Shallow	Deep
Depth (m)	150 – 450	450 – 775
T_{tot} (m^2/s)	$5x10^{-7}$	$2.8x10^{-6}$
I (m^2/s)	$6.3x10^{-7}$	$3.5x10^{-6}$
r_i (m)	12	12
P_{avg} (GL m)	2.3	5.4

845

846

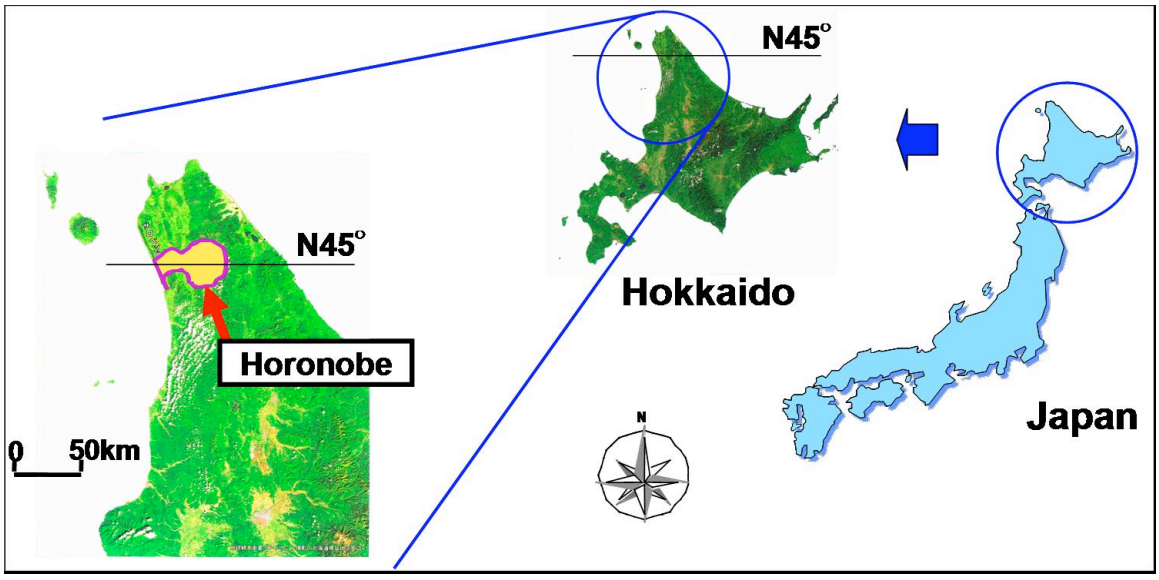

Figure 1. Location map of Horonobe.

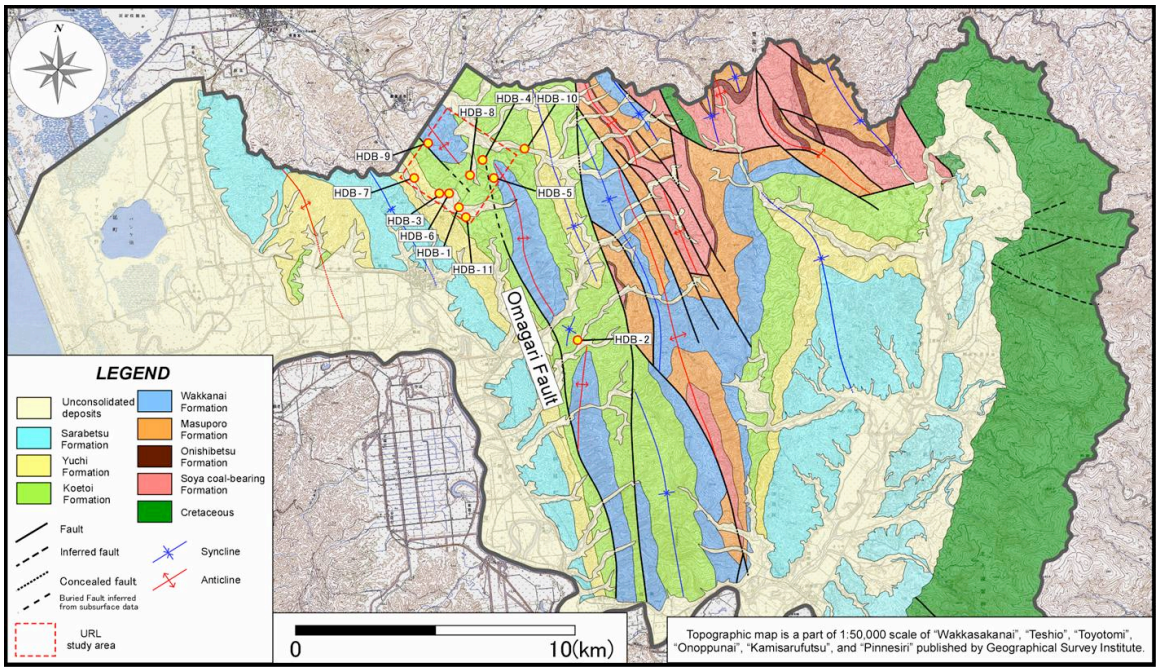

Figure 2. Surface geologic map of Horonobe town.

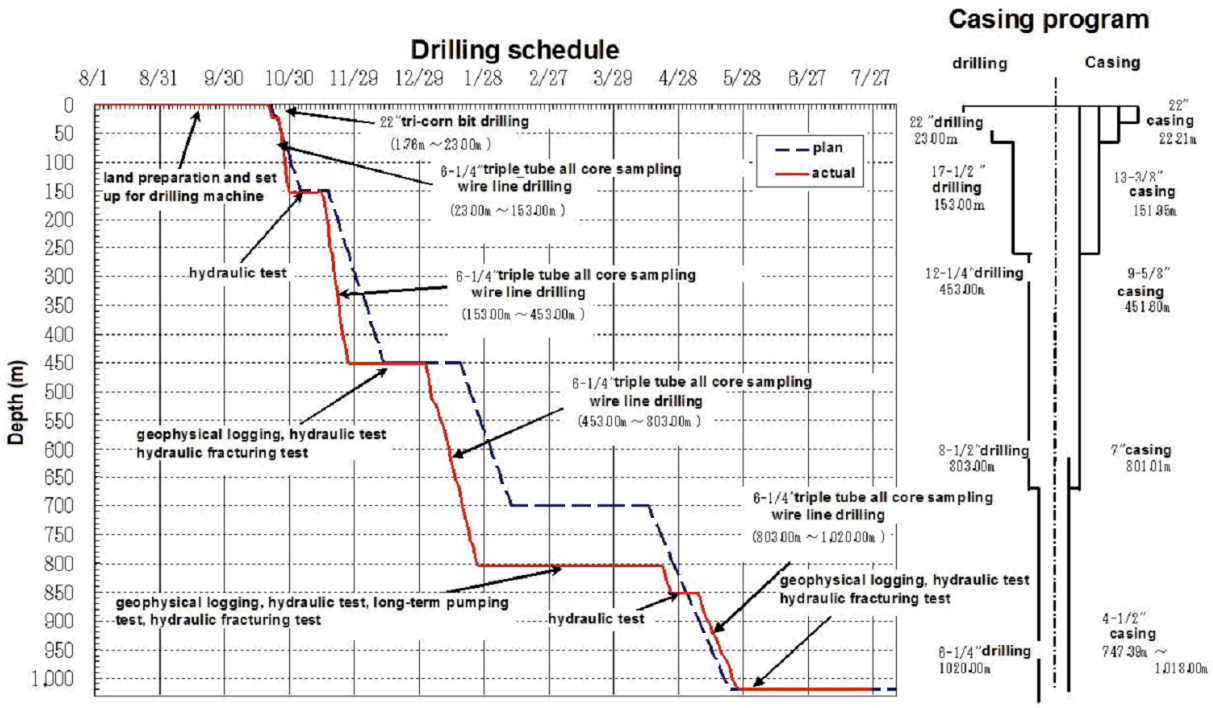

Figure 3. Drilling schedule and casing program for Well HDB-11.

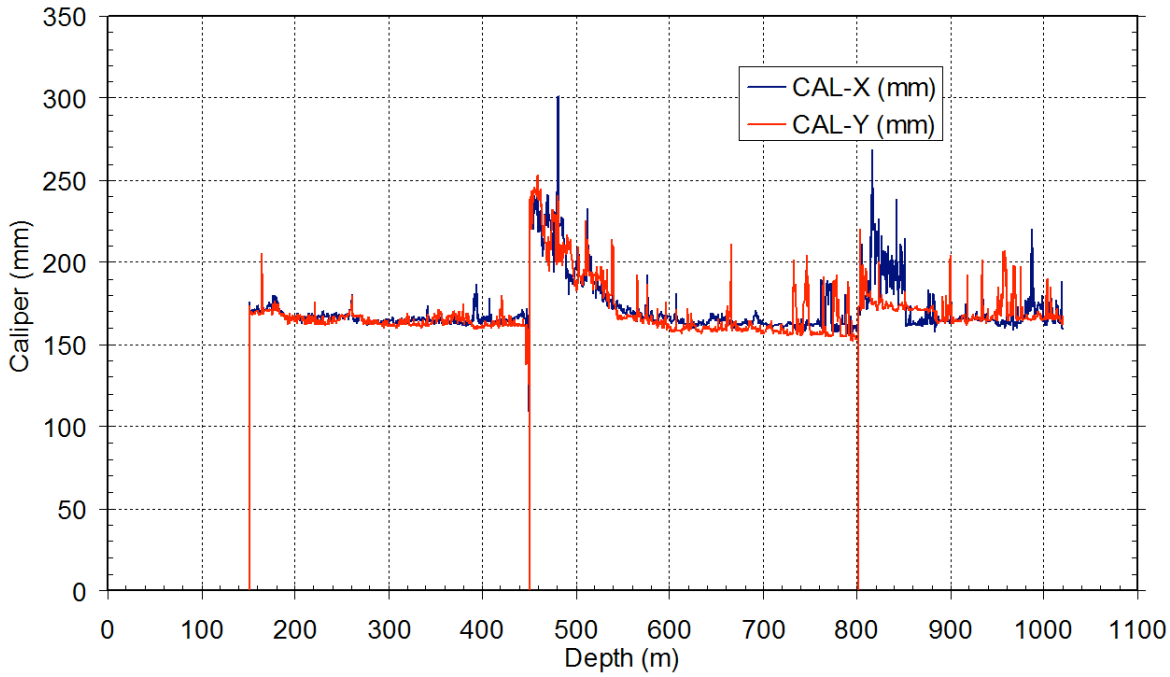

Figure 4. Caliper log for Well HDB-11.

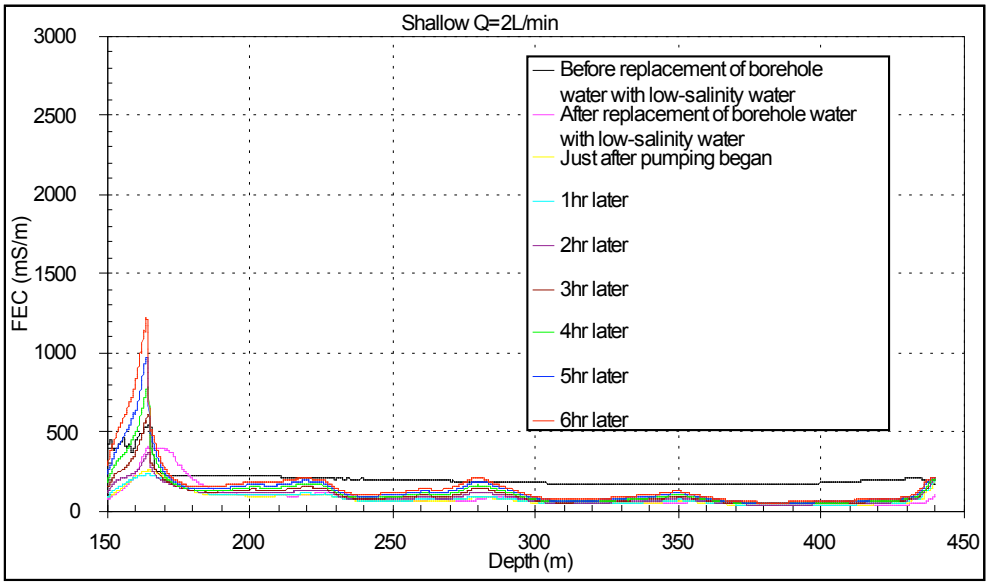

857

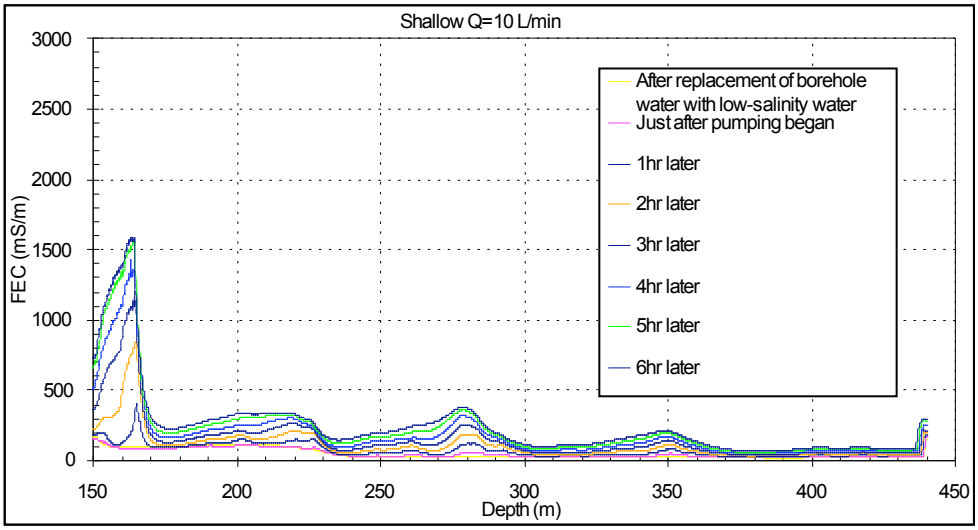

858

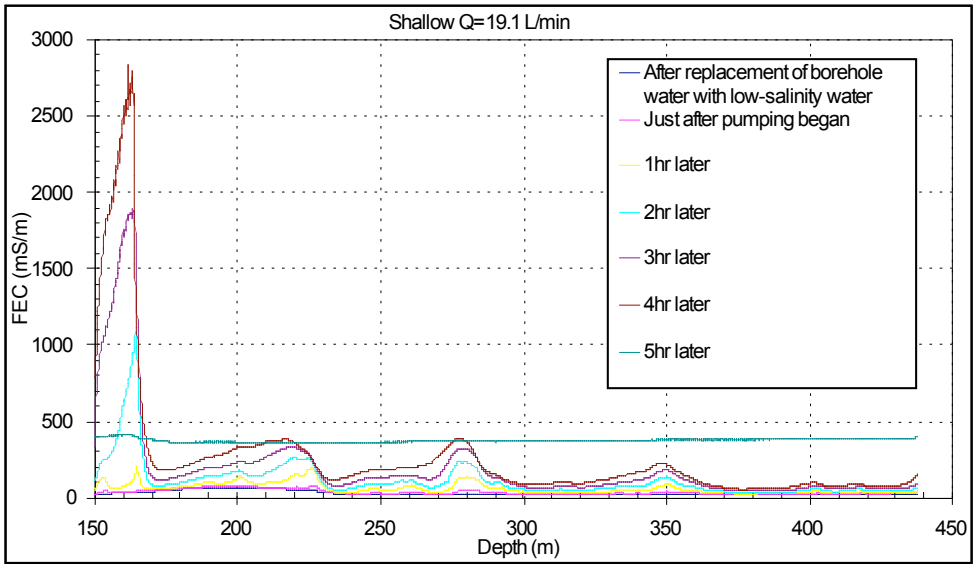

859

860 Figure 5. Original FEC data for shallow zone.

861

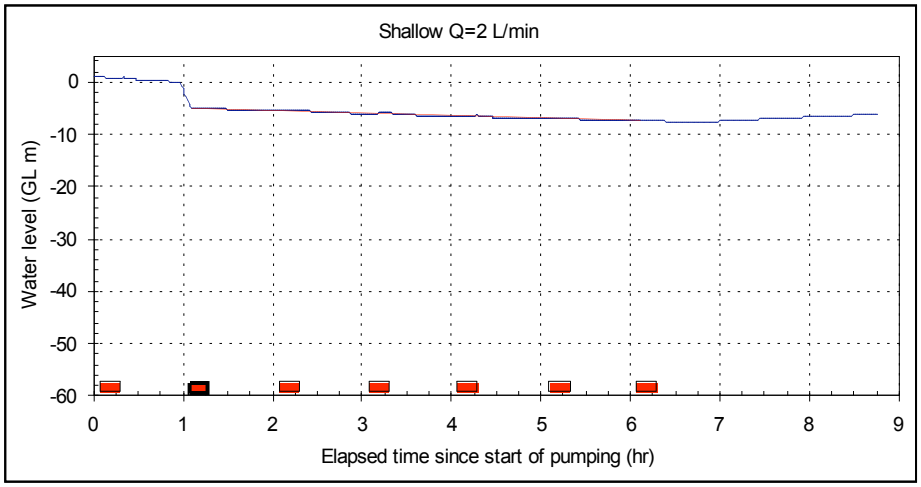

861

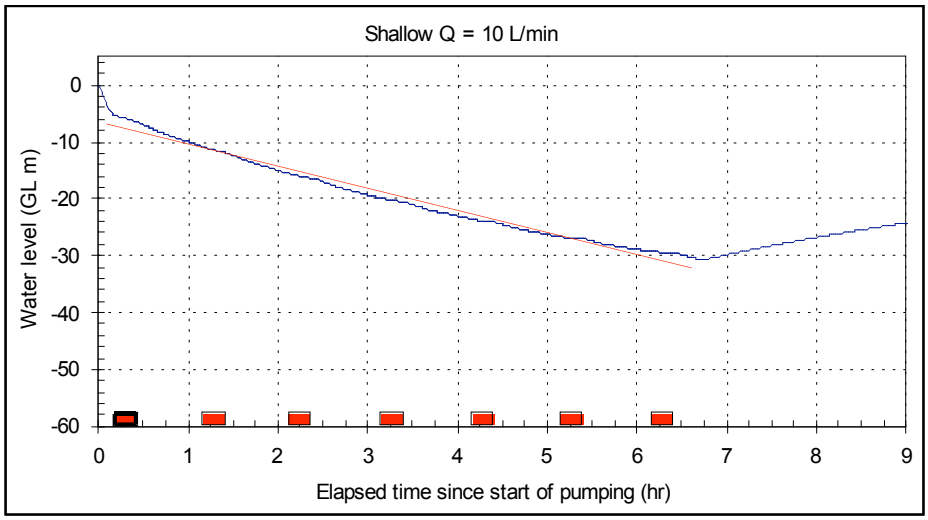

862

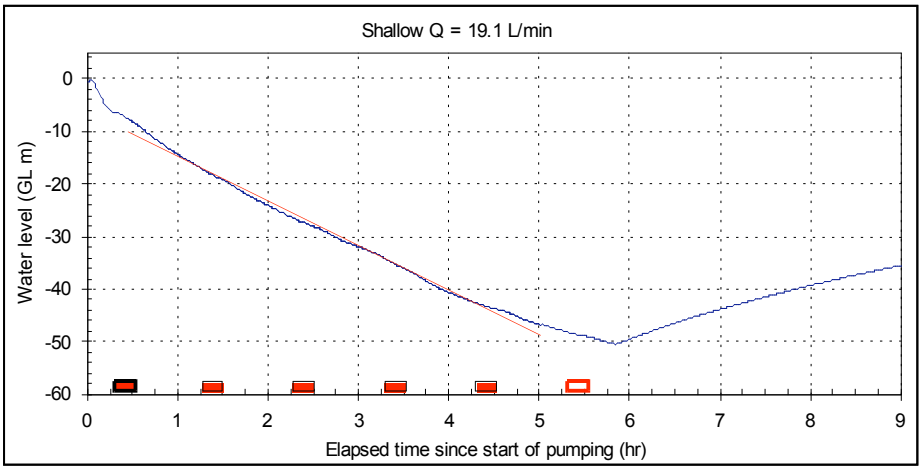

863

864 Figure 6. Water-level data obtained during FEC logging of shallow zone (blue curve)
865 and linear fit of the portion of the curve obtained while usable FFEC logs were collected
866 (red line). Times at which FFEC logging occurred are shown as red boxes. The black-
867 outlined box identifies the profile used as the initial condition for the BORE II model.
868 The open box indicates an FEC profile that could not be used for analysis.

869

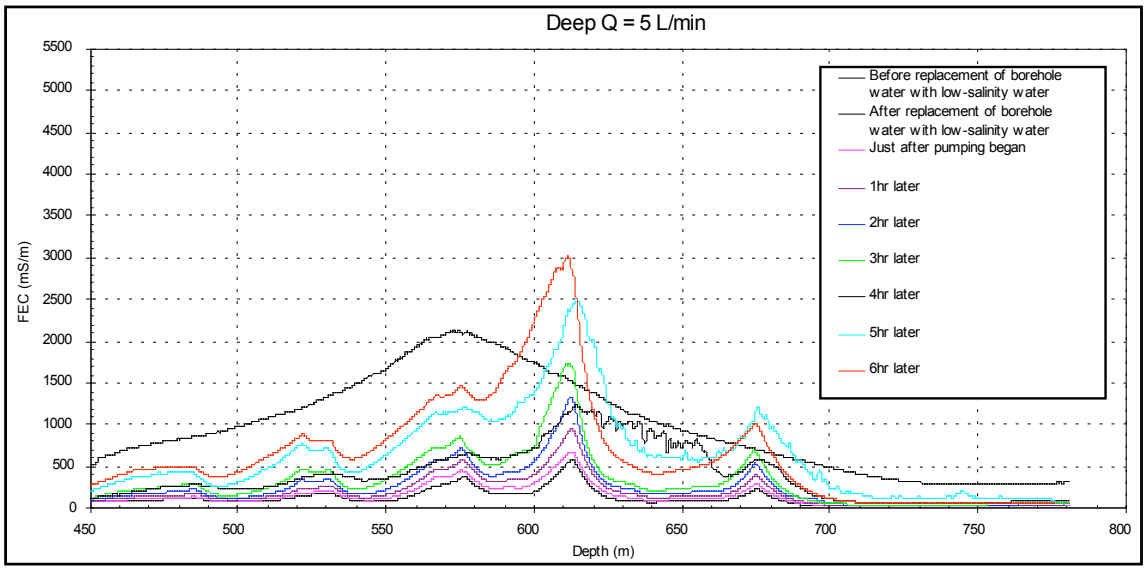

870

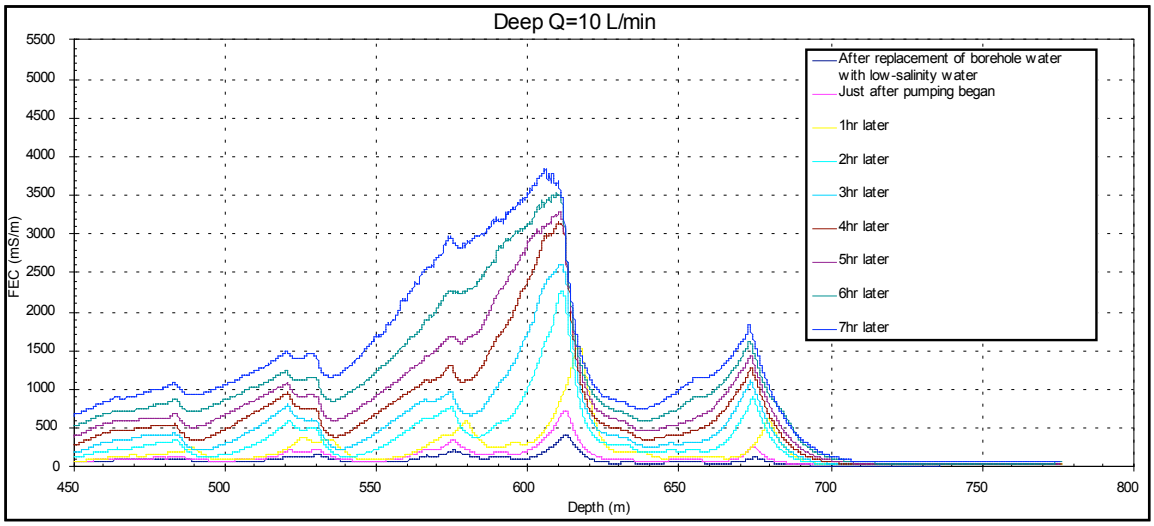

871

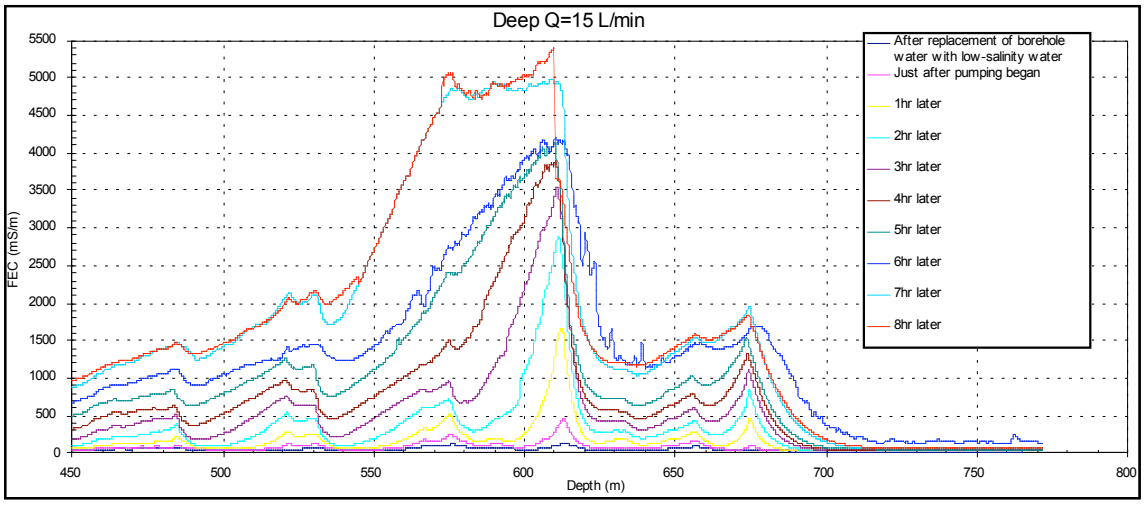

872

873 Figure 7. Original FEC data for deep zone.

874

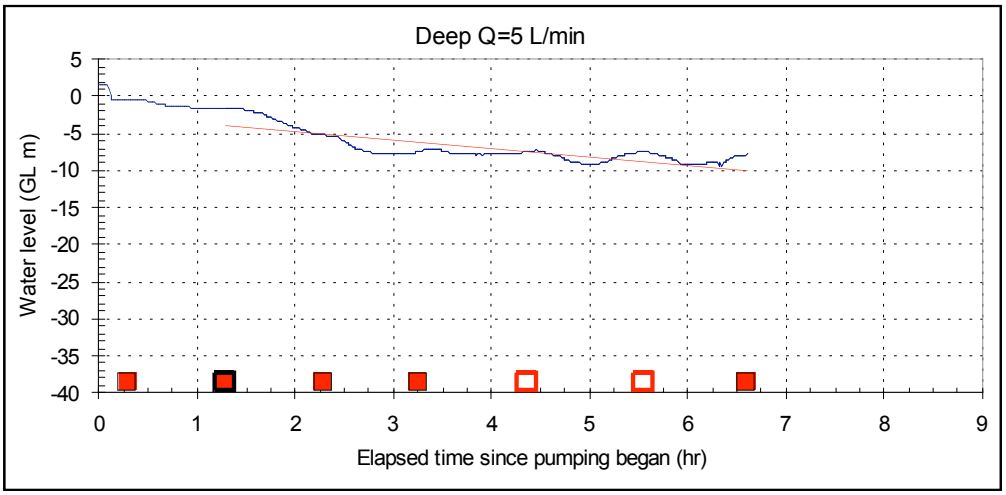

874

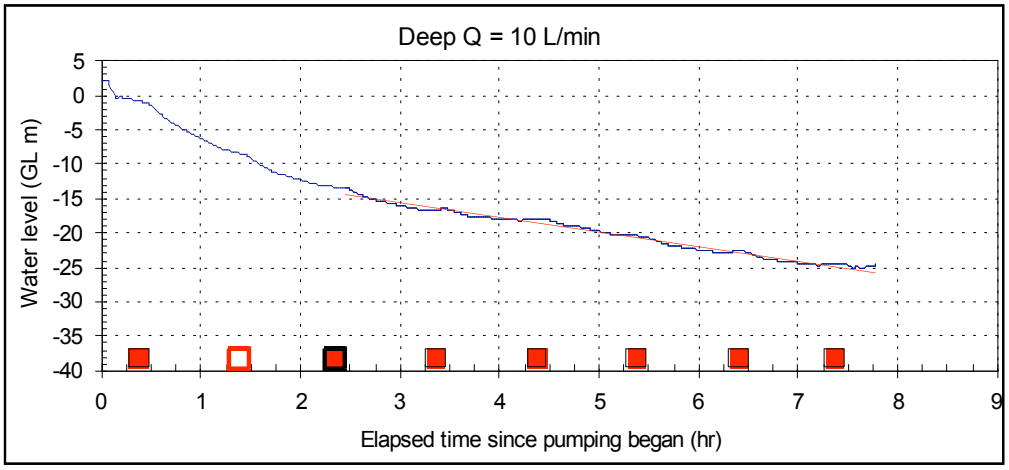

875

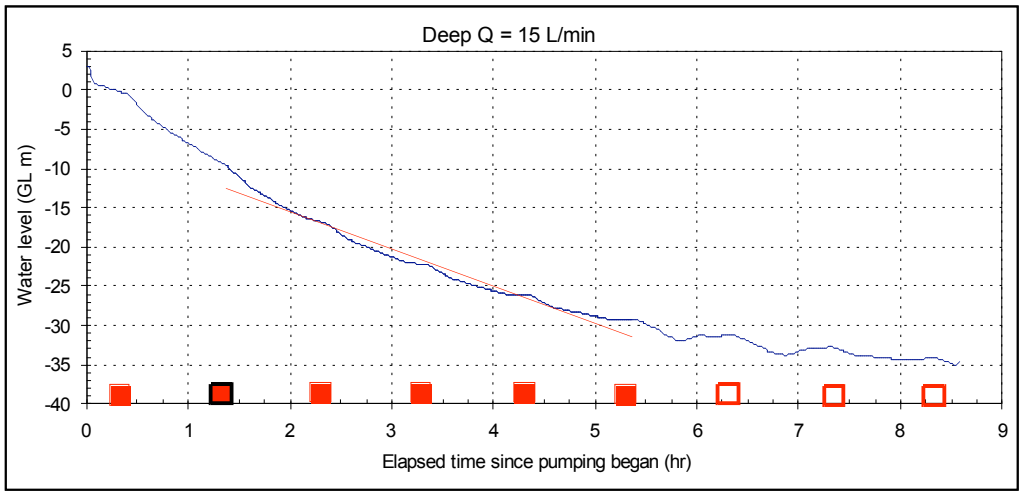

876
877 Figure 8. Water-level data obtained during FEC logging of deep zone (blue curve) and
878 linear fit of the portion of the curve obtained while usable FFEC logs were collected (red
879 line). Times at which FFEC logging occurred are shown as red boxes. The black-
880 outlined box identifies the profile used as the initial condition for the BORE II model.
881 The open boxes indicate FEC profiles that could not be used for analysis.
882

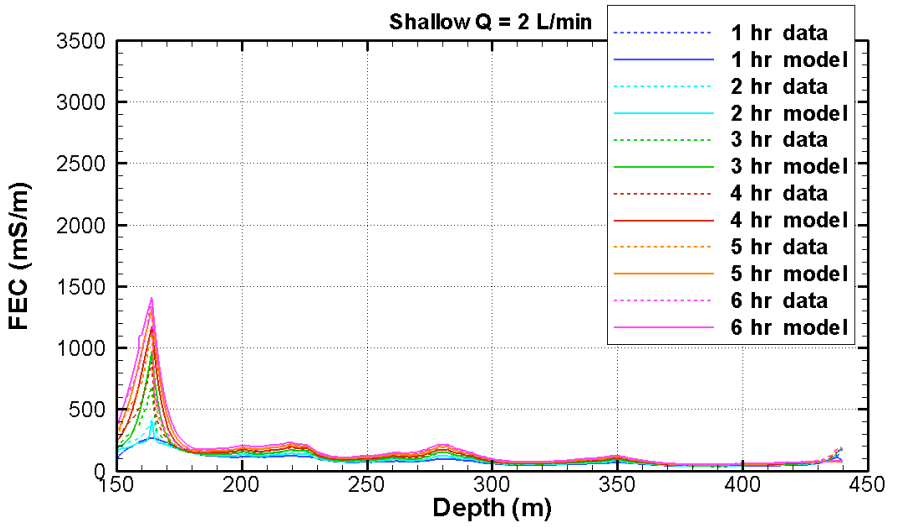

882

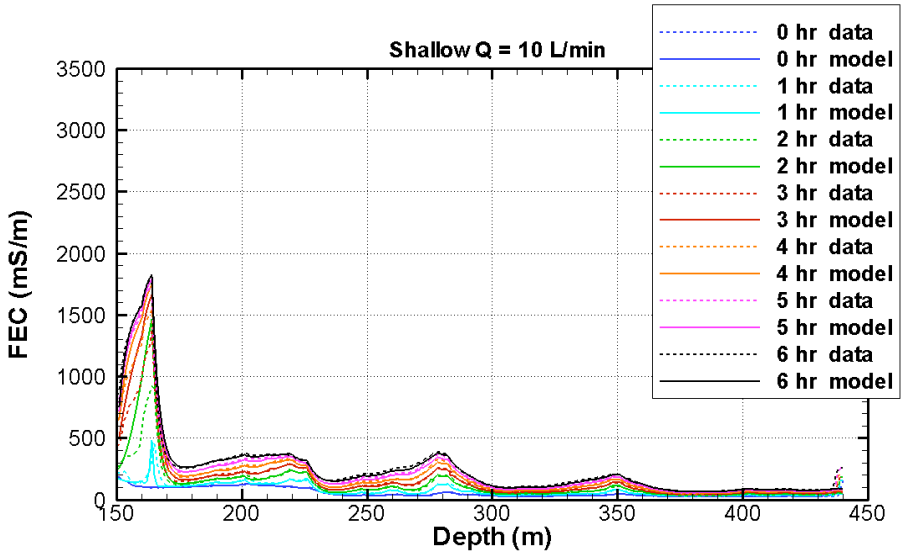

883

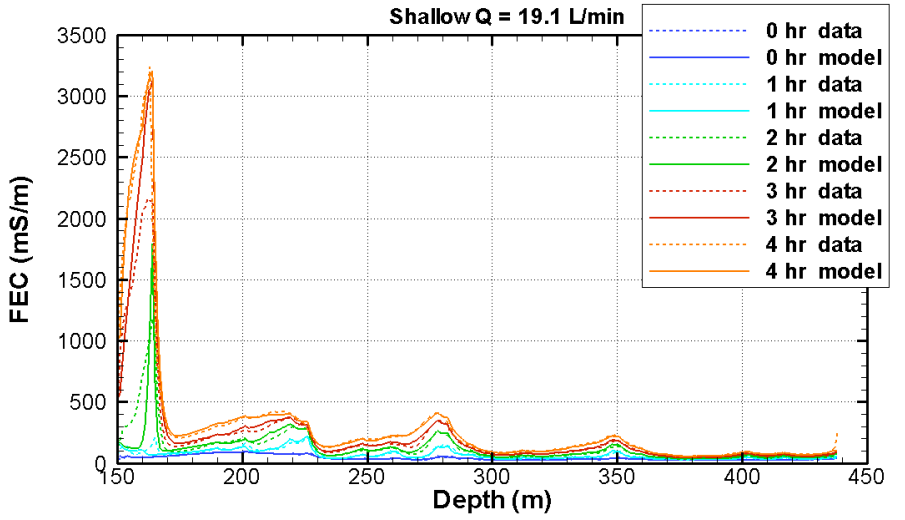

884
885 Figure 9. Processed FEC data and model fit for shallow-zone tests.
886

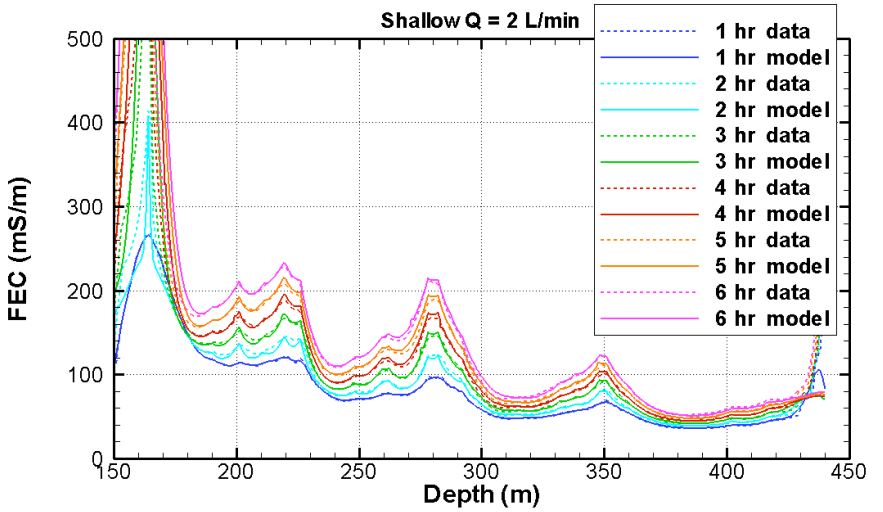

886

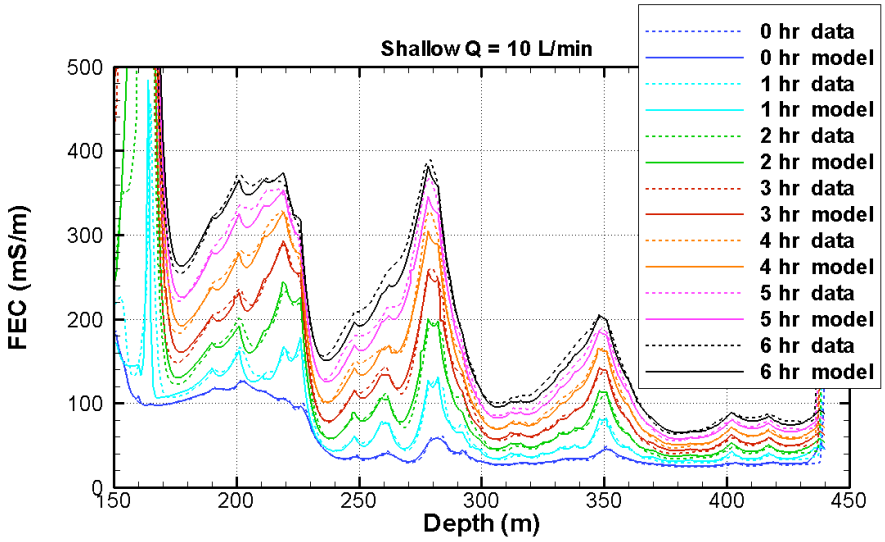

887

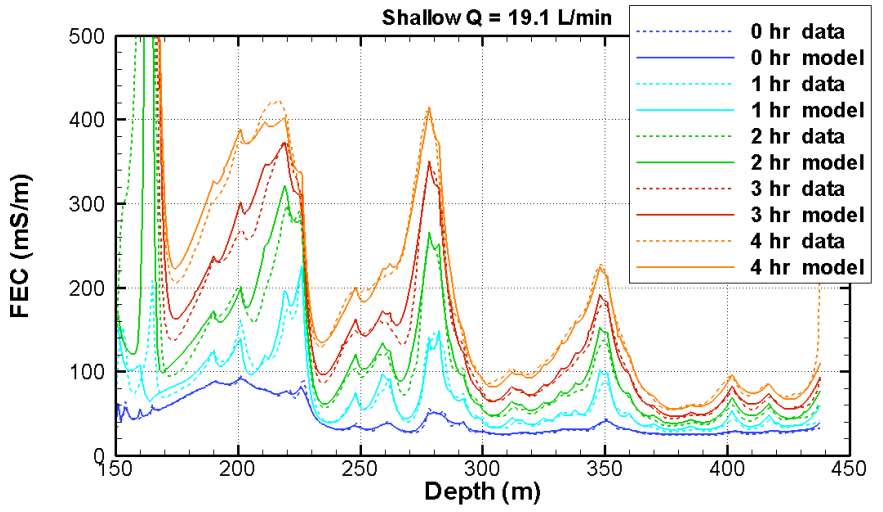

888
889 Figure 10. Processed FEC data and model fit for shallow-zone tests. Expanded scale to
890 show details of small peaks.
891

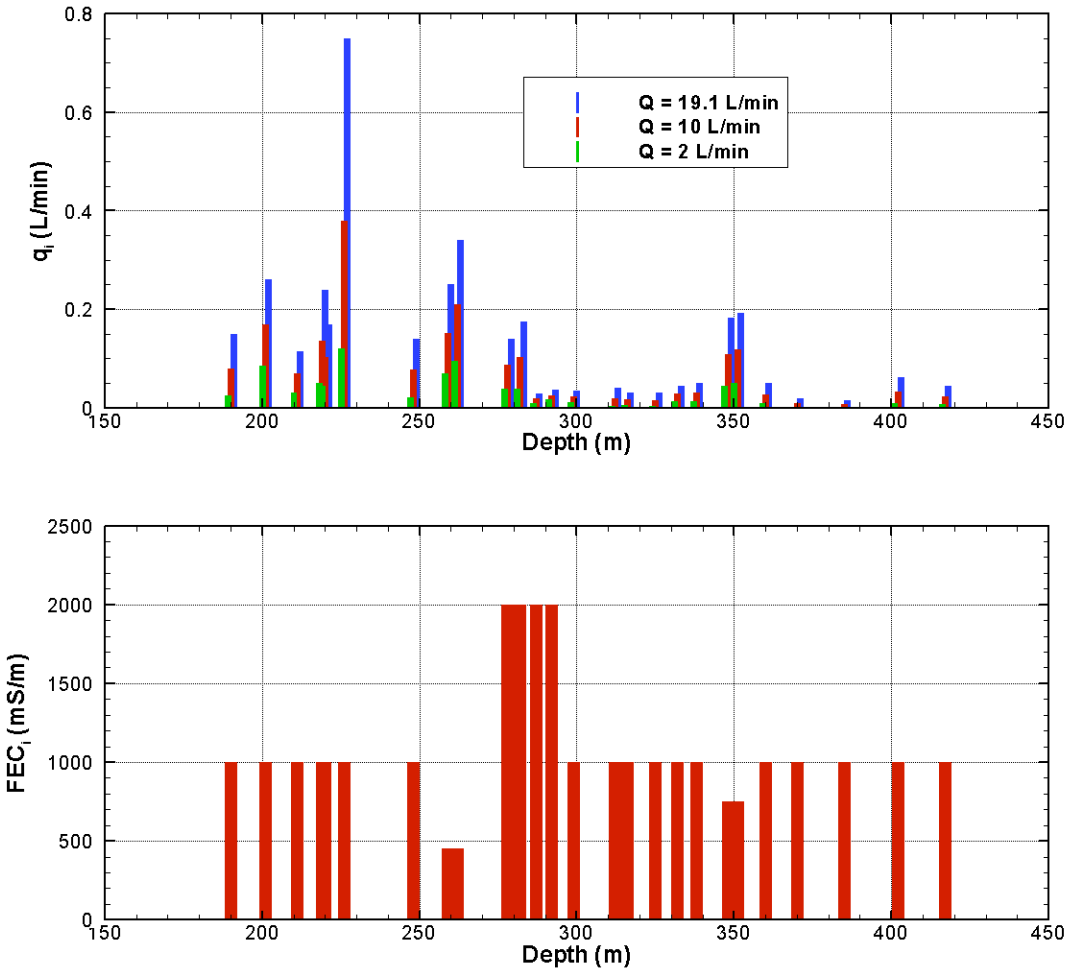

Figure 11. Direct-fit results for feed-point strength q_i and salinity (expressed as FEC in mS/m) for shallow-zone tests.

894

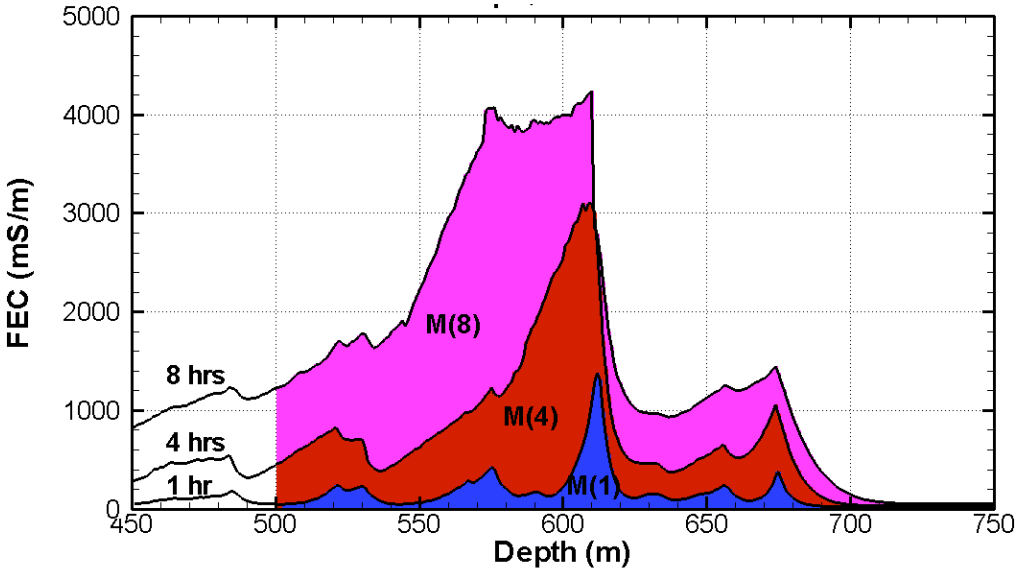

895

896 Figure 12. Schematic of the $M(t)$ method for the depth interval 500-750 m.

897

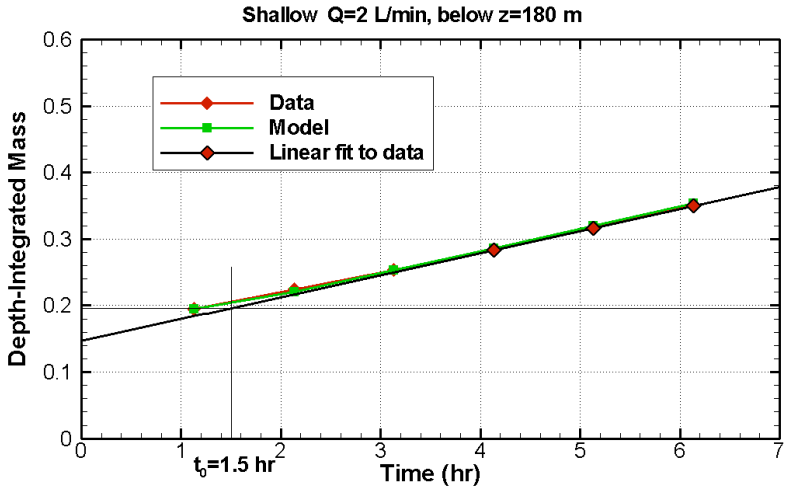

897

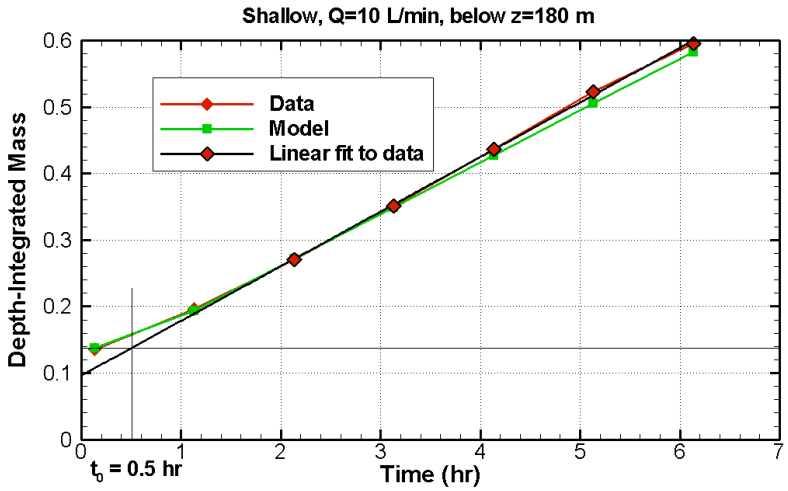

898

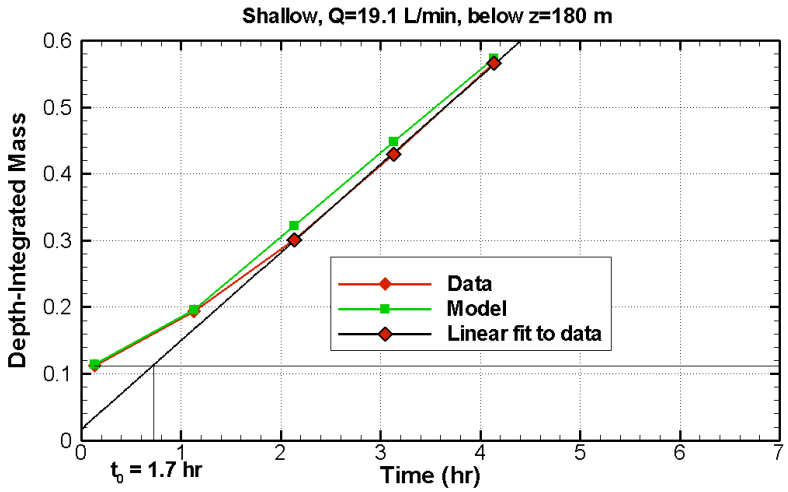

899
900 Figure 13. $M(t)$ results for shallow-zone tests. The first FEC profile is used as the model
901 initial condition for each test. The vertical line shows the average t_0 for all the feed
902 points, determined as the time at which a linear extrapolation of $M(t)$ intersects the mass
903 in place at the initial condition (horizontal line).

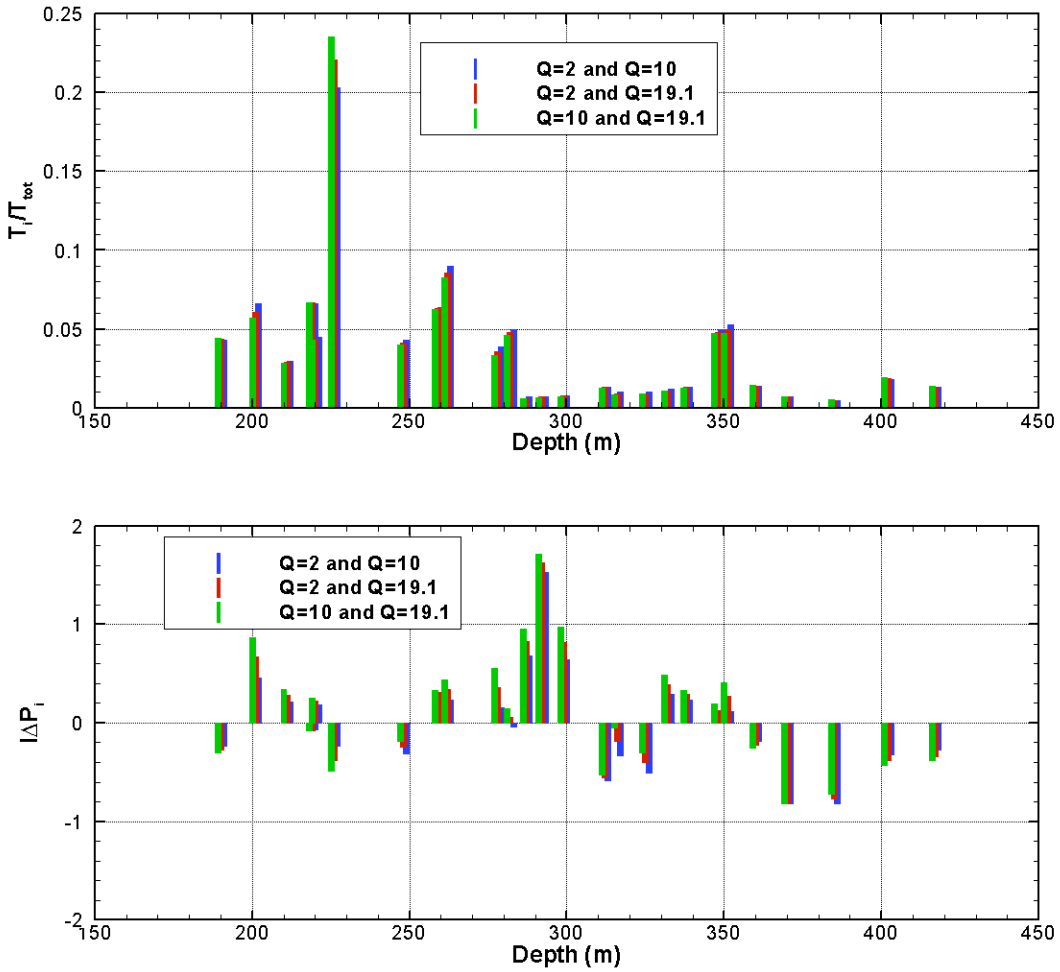

Figure 14. Multi-rate results T_i/T_{tot}, $I\Delta P_i$ for shallow-zone tests.

906

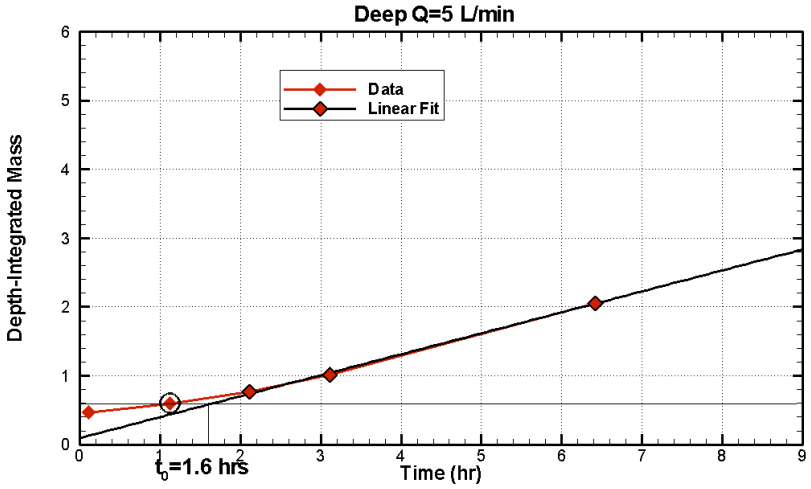

907

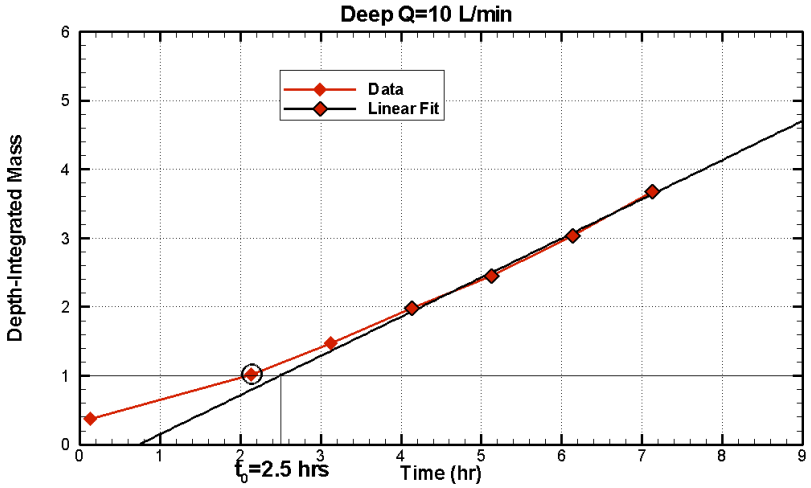

908

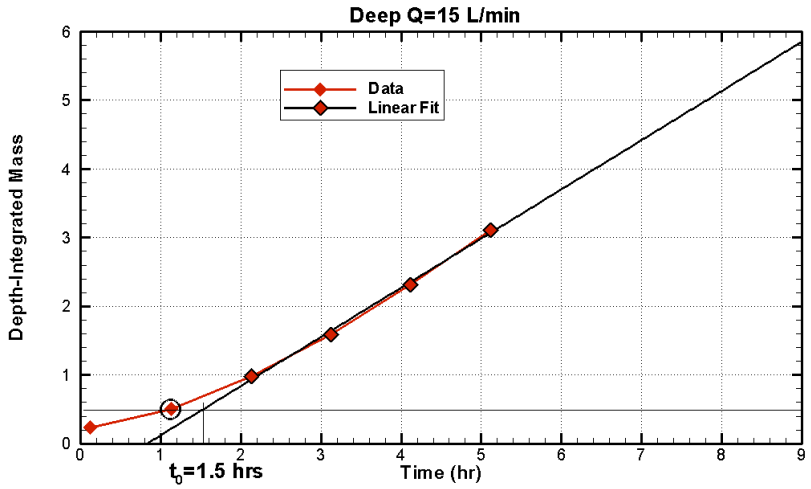

909 Figure 15. $M(t)$ results for deep-zone tests. The FEC profile used as the model initial
910 condition is circled. The intersection of the mass in place at the initial conditions
911 (horizontal line) and the linear fit to $M(t)$ determines t_0.
912

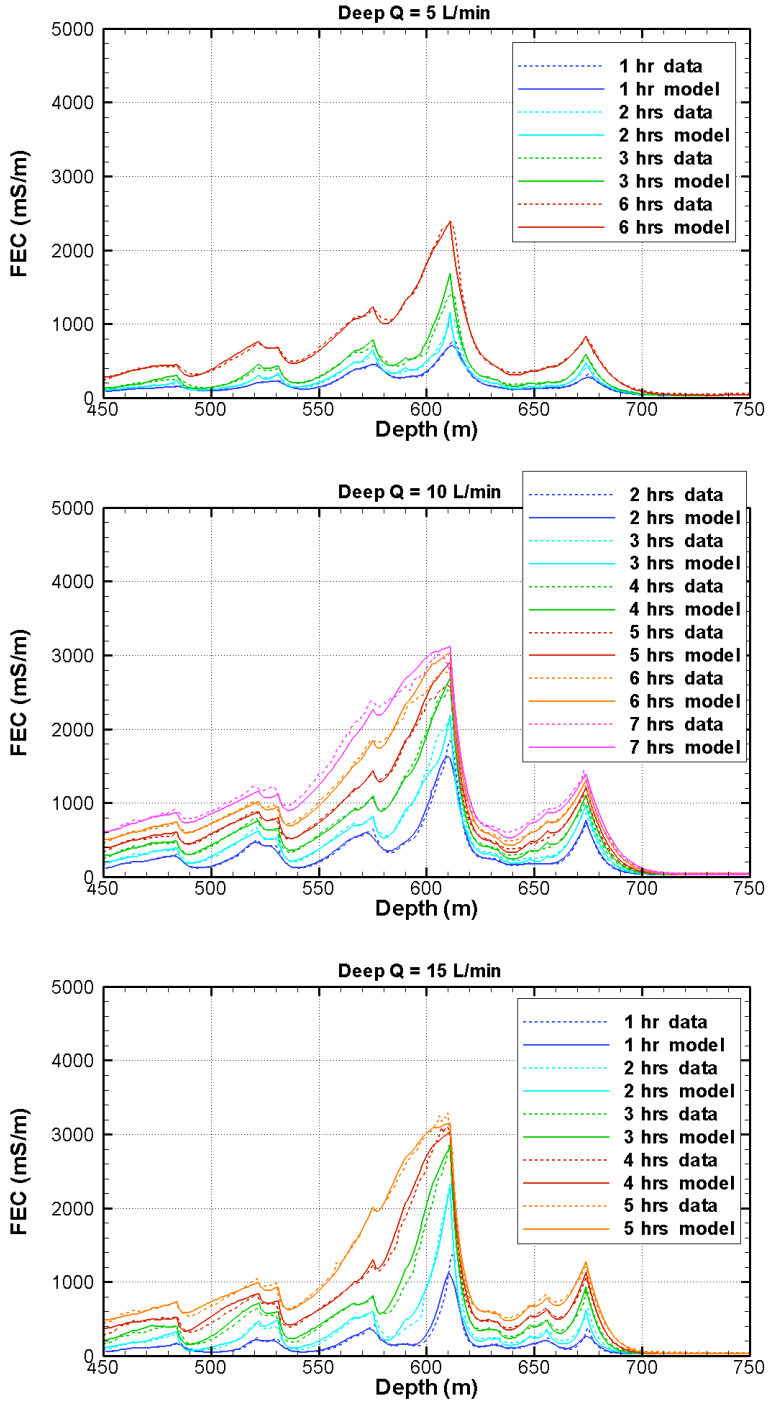

Figure 16. Processed FEC data and model fit for deep-zone tests.

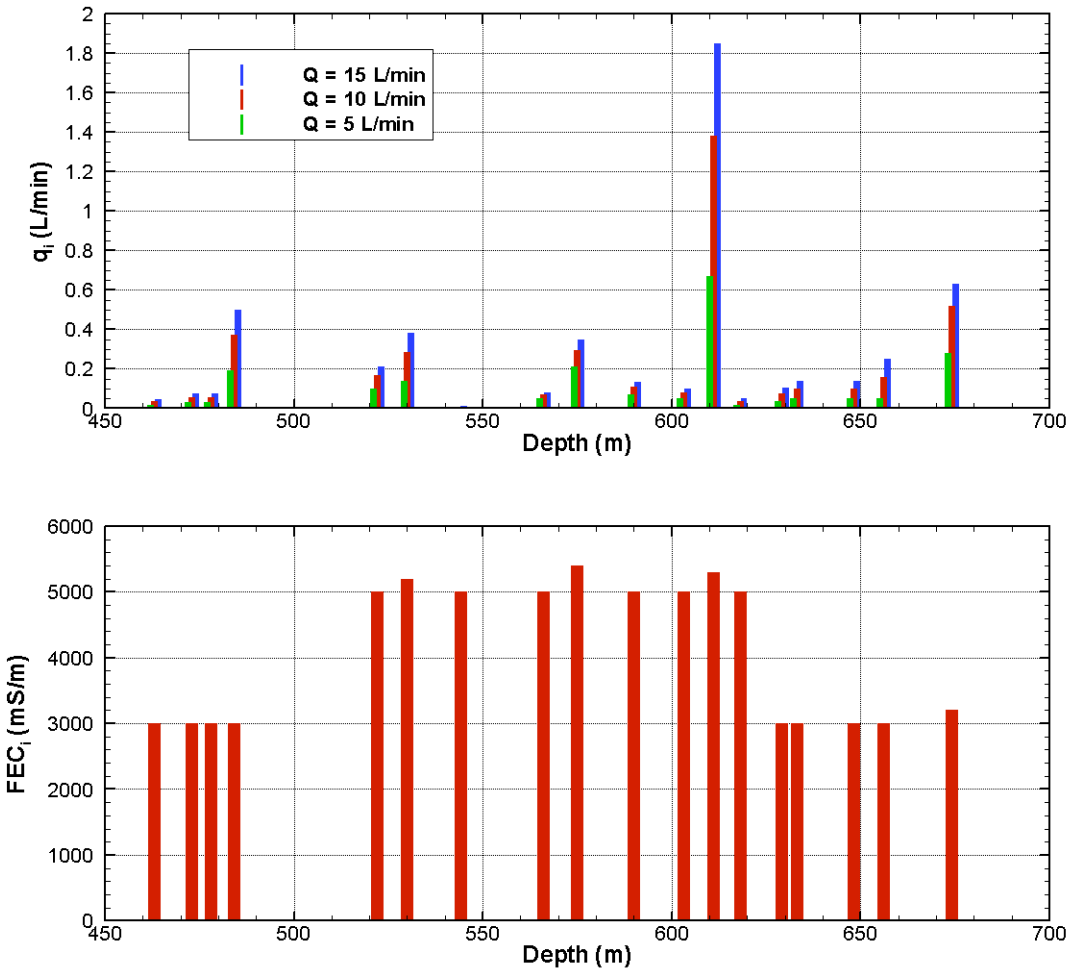

Figure 17. Direct-fit results for feed-point strength q_i and salinity (expressed as FEC in mS/m) for deep-zone tests.

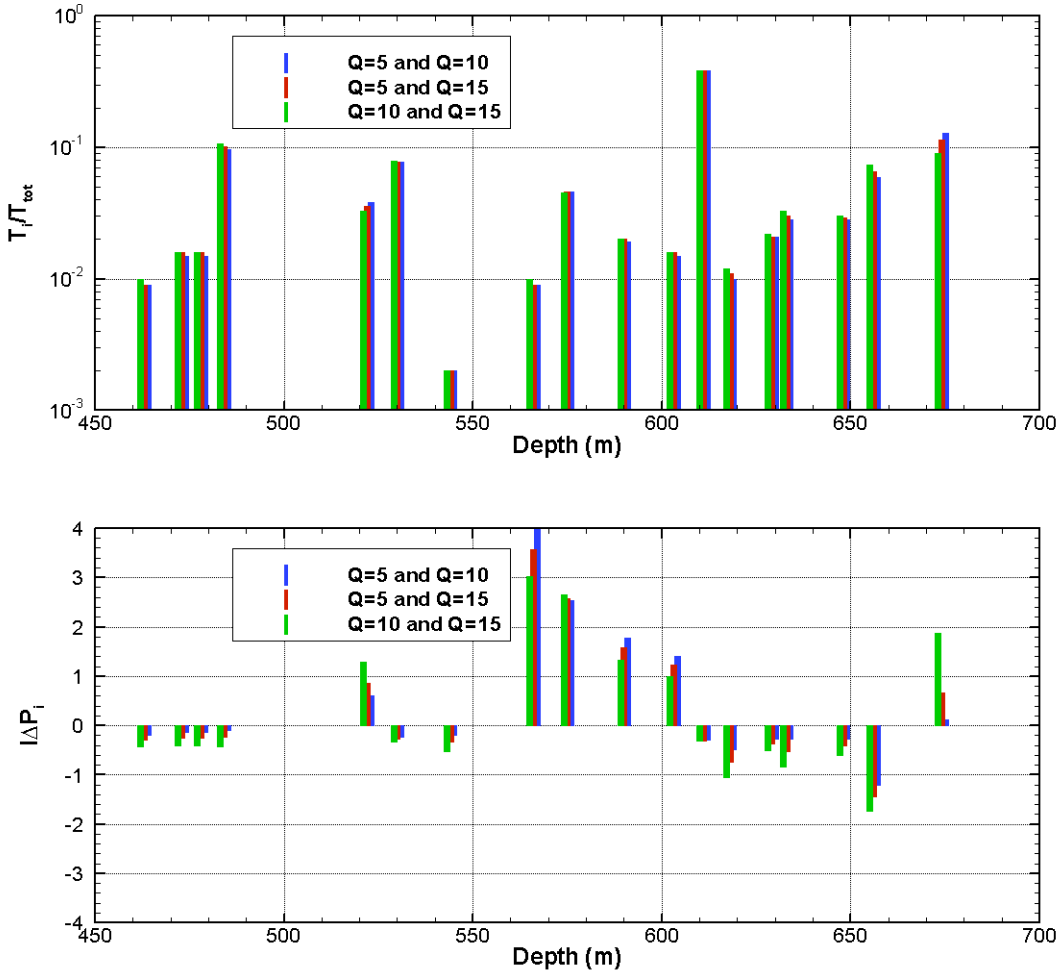

Figure 18. Multi-rate results T_i/T_{tot}, $I\Delta P_i$ for deep-zone tests.

921

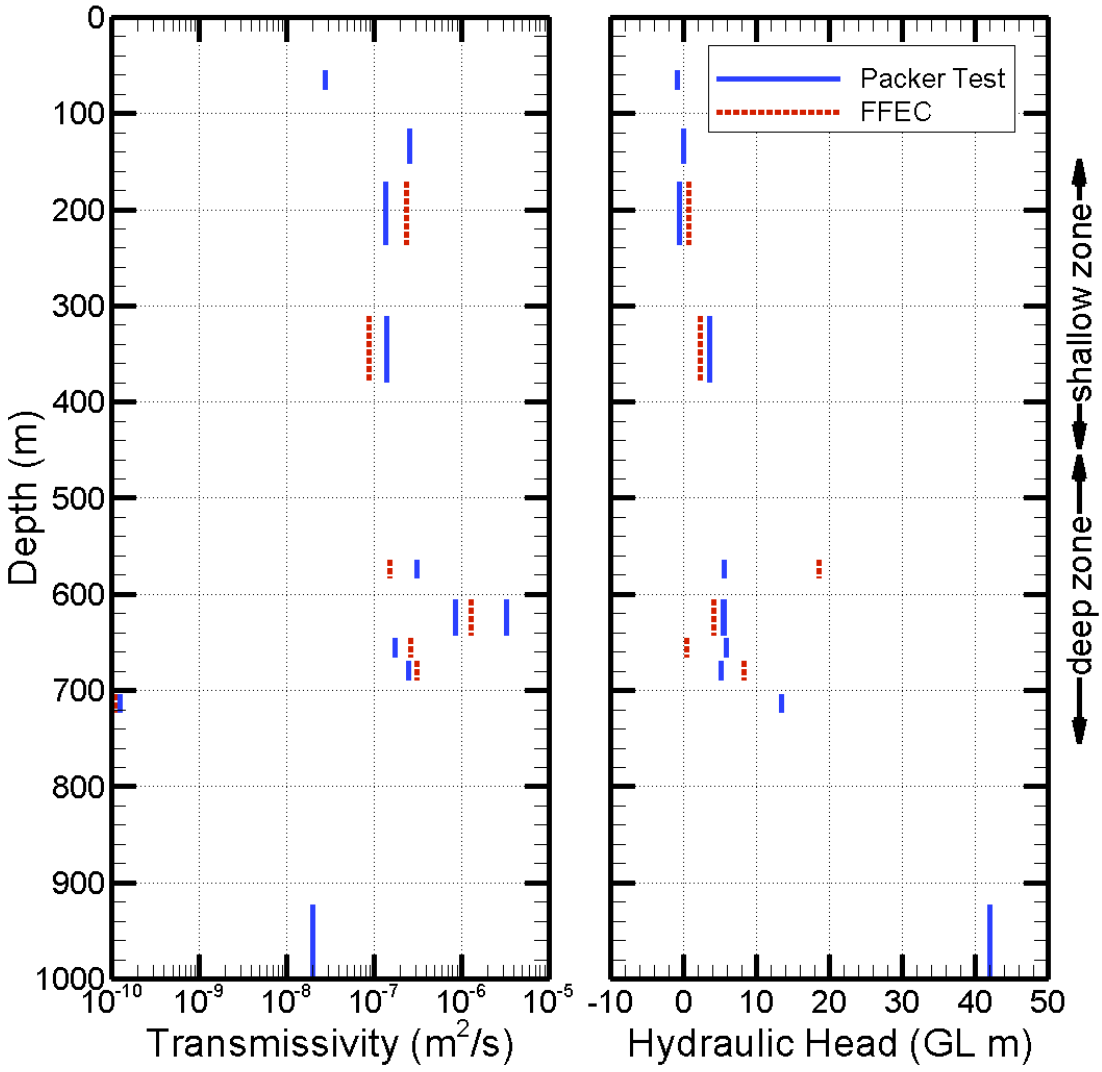

922
923 Figure 19. Comparison of packer-test results (blue) and values inferred from multi-rate
924 flowing FEC logging (red) for transmissivity and pressure head for selected intervals in
925 Well HDB-11.
926

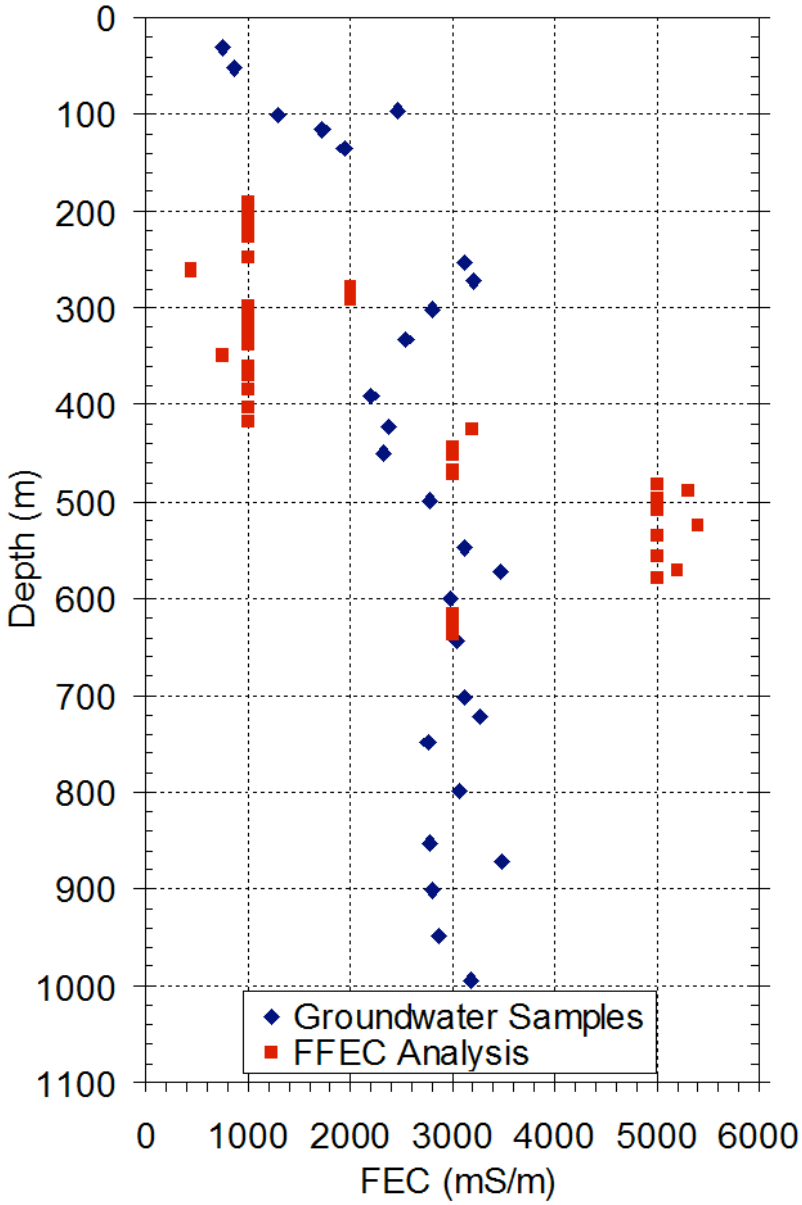

926

927 Figure 20. Comparison of FEC values inferred from FFEC logging and electric
928 conductivity from groundwater squeezed from core samples from Well HDB-11.